

SUPPORT TO MIPAS PHASE E Activities
under contract by ABB Bomem Inc.

**Complete in-flight detector non-linearity characterisation of
MIPAS/Envisat**

TN

**Michelson Interferometer for Passive
Atmospheric Sounding**

Authors: M. Birk, G. Wagner

Doc. No.:
Issue: 1 A
Date: 18.10.2010

1 Contents

1	Contents	2
2	Reference documents	3
3	Introduction.....	3
4	Data compilation of all IF4, IF16	3
5	Gainratio investigation	7
6	Fits of all available IF4/IF16 sequences	8
7	New method	11
8	Modifications and tests.....	15
8.1	Reduced phase resolution in modelled spectra for more symmetric residuals	15
8.2	Improved selection of interferograms, DS added	15
8.3	Improved convergence criterion	15
8.4	Fits for various initial guesses and selection of best result	15
8.5	Non-linearity characterisation for B1 and B2 with a quadratic term only	16
8.6	No 0th order out-of-band artifact for B2	16
8.7	Radiance contrast difference.....	18
8.8	Reproducibility.....	18
8.9	Dependence on out-of-band artifacts.....	20
8.10	Investigation of non-vanishing residuals for quadratic out-of-band artifacts..	27
9	Calculation of effect of ice and instrument temperature	28
10	Results of single orbit fits.....	29
11	Further data reduction.....	32
12	Error analysis.....	40
12.1	Error due to modulation efficiency	41
12.2	Intrinsic model error.....	41
12.3	Out-of-band selection error	41
12.4	Regression error.....	41
12.5	ADCmaxmin error.....	41
13	Proposal for level 2 quality check.....	42
14	Summary	42

2 Reference documents

[RD1] Enhanced Analysis of MIPAS Radiometric Performance Using In-Flight Calibration Data, Change #1 of contract 16150/02/NL/SF, TN1 + TN2

[RD2] Improvement of DLR detector non-linearity characterisation for MIPAS/Envisat, contract by ABB Bomem Inc., Offer-No.: 3 400 178

[RD3] Noise analysis of MIPAS/ENVISAT in-flight measurements, contract by IMK, contract number 315/20228879/IMK

[RD4] Investigation of detector, optics, and CBB degradation from commissioning phase to April 2009, contract by ABB Bomem Inc.

[RD5] Influence of ice contamination and instrument temperature change on detector non-linearity, contract by ABB Bomem Inc.

3 Introduction

An improved detector non-linearity characterisation method was presented in [RD2] applying the “DC zero” method. The method was only applied to data from the commissioning phase and made use of IF4 (nominal mode CBB measurements at different blackbody temperatures) and IF16 (raw data mode CBB, DS, and scene measurements) data. The primary outputs were quadratic and cubic detector non-linearity coefficients and the modulation efficiency. The detector curve was converted into “BOMEM parameters” relating the derivative of the detector curve to ADC_{max} values which are part of the level 1 product.

The present document shows the application of this method to all available characterisation data. The method was refined allowing investigation of all available IF16 data sets. The accuracy of the method was investigated. The influences on the detector non-linearity throughout the mission were characterised and could be parameterised by means of linear regression. This allows calculating the appropriate non-linearity correction for any orbit throughout the mission.

4 Data compilation of all IF4, IF16

All measured IF4 and IF16 data sets are listed in table 1. IF4 measurements are rare compared to IF16 measurements since changing CBB temperature takes a long time due to the thermal time constant and a considerable amount of measurement time is required. There are 5 IF4 sequences available. In case of IF16 only those sequences including scene, CBB, and DS measurements can be utilised. Furthermore, data sets of consecutive orbits do not yield extra information. Finally, there are 21 IF16 sets available so far, 20 sets have been analysed as marked in Table 1.

Table 1. Compilation of IF4 and IF16 sequences throughout mission.

Date	Orbit	In-Flight Calibration	Acquisition Status at ESA	Remark	IF16 analysis
22.06.2002	1621	IF4	Acquired and stored		
22.06.2002	1623	IF4	Acquired and stored		
22.06.2002	1627	IF4	Acquired and stored		
23.06.2002	1636	IF4	Acquired and stored		
26.06.2002	1680-1681	IF16	Acquired and stored		x
15.09.2002			DECONTAMINATION		
27.02.2003	5203 - 5204	IF16	Acquired and stored		x
01.04.2003			DECONTAMINATION		
07.04.2003	5764	IF16	Acquired and stored	6 days after decont.	x
08.04.2003	5773 - 5780	IF4	Acquired and stored		
09.04.2003	5787 - 5794	IF4	Acquired and stored		
10.04.2003	5800 - 5809	IF4	Acquired and stored		
11.04.2003	5821 - 5822	IF16	Acquired and stored	DS/CBB missing	
02.07.2003	6990 - 6991	IF16	Acquired and stored		x
04.09.2003	7908 - 7909	IF16	Acquired and stored	DS/CBB missing	
06.11.2003	8808 - 8809	IF16	Acquired and stored	DS/CBB missing	
02.02.2004			DECONTAMINATION		
09.02.2004	10173 - 10174	IF16	Acquired and stored	7 days after decont.	
10.02.2004	10180 - 10183	IF4	Acquired and stored		
11.02.2004	10196 - 10198, 10202	IF4	Acquired and stored		
12.02.2004	10209 - 10211	IF4	Acquired and stored		

13.02.2004	10230 - 10231	IF16	Acquired and stored		x
07.02.2005	15377 - 15378	IF16	Acquisition failure (OAR 2015)	DS/CBB missing	
25.04.2005	16486 - 16487	IF16	Acquisition failure (OAR 2015)	max. contamination	x
01.06.2005			DECONTAMINATION(big)		
29.08.2005	18286 - 18287	IF16	Acquisition failure (OAR 2015)		
28.10.2005	19146 - 19147	IF16	Acquired and stored		x
10.03.2006	21052 - 21053	IF16	Acquisition failure (OAR 2015)		
11.04.2006			PLSOL		
05.06.2006	22292 - 22293	IF16	Acquisition failure (OAR 2015)		
07.09.2006			DECONTAMINATION		
28.11.2006			PLSOL		
10.01.2007	25426 - 25427	IF16	Acquired and stored		x
01.04.2007	26589 - 26590	IF16	Acquired and stored		x
29.05.2007			DECONTAMINATION		
21.07.2007	28179 - 28180	IF16	Acquired and stored		x
17.10.2007			DECONTAMINATION		
24.10.2007	29538 - 29539	IF16	Acquired and stored	7 days after decont.	x
26.10.2007	29558 - 29562	IF4	Acquired and stored		
27.10.2007	29572 - 29576	IF4	Acquired and stored		
28.10.2007	29591 - 29595	IF4	Acquired and stored		
28.10.2007	29596 - 29597	IF16	Acquired and stored	DS/CBB missing	
03.12.2007			PLSOL		
21.03.2008	31671 - 31672	IF16	Acquired and stored		x
29.04.2008	32229 -	IF16	Acquired and stored	before decont.	x

	32230				
30.04.2008			DECONTAMINATION		
09.05.2008	32372 - 32373	IF16	32372: Acquired and stored. 32373: Not acquired due to PDS problem	10 days after decont.	
21.05.2008	32547 - 32548	IF16	Acquired and stored	sideways	x
31.07.2008	33559 - 33560	IF16	Lost due to instrument unavailability (MCMD acknowledgment error)		
19.09.2008	34276 - 34277	IF16	Acquired and stored		x
05.10.2008			DECONTAMINATION		
07.12.2008	35406 - 35407	IF16	Acquired and stored		x
20.02.2009	36480 - 36481	IF16	Acquired and stored		x
21.04.2009	37339 - 37340	IF16	Acquired and stored	before decont.	x
22.04.2009			DECONTAMINATION		
30.04.2009	37469 - 37470	IF16	Acquired and stored	8 days after decont.	x
03.11.2009	40144 - 40145	IF16	Acquired and stored	DS/CBB missing	
04.11.2009			DECONTAMINATION		
12.11.2009	40274 - 40275	IF16	Acquired and stored		x
13.11.2009	40279 - 40283	IF4	Acquired and stored		
15.11.2009	40316 - 40320	IF4	Acquired and stored		
17.11.2009	40353 - 40357	IF4	Acquired and stored		
19.11.2009	40371 - 40375	IF4	Acquired and stored		
21.11.2009	40398 - 40399	IF16	*Level1a.0 file missing		

5 Gainratio investigation

Gainratios between different orbits were investigated throughout the mission. Results are summarised in [RD4]. D channel gainratios were found to be unchanged within 1% throughout the mission, indicating that there is no aging of CBB, optics, and channel D detectors. Channel C gainratios showed occasionally discrepancies up to 3%, perhaps linked to ice contamination. Some IF16 channel D gainratios showed deviations from 1 which could be linked to temperature sensor readout overflow. The gainratios were tuned to 1 by adjusting the CBB temperature. All IF4 CBB temperatures were qualified by inspecting channel D gainratios and tuned accordingly where necessary. The resulting temperatures were used to obtain A and B channel gainratios. The photoconductive channels showed degradation with time (see [RD4]). The degradation was documented for all IF16 sequences for the A2 channel (forward sweeps). Ratios with orbit 1680 were formed in a spectral region without ice absorption and are shown in Figure 1. They exhibit almost linear time dependence.

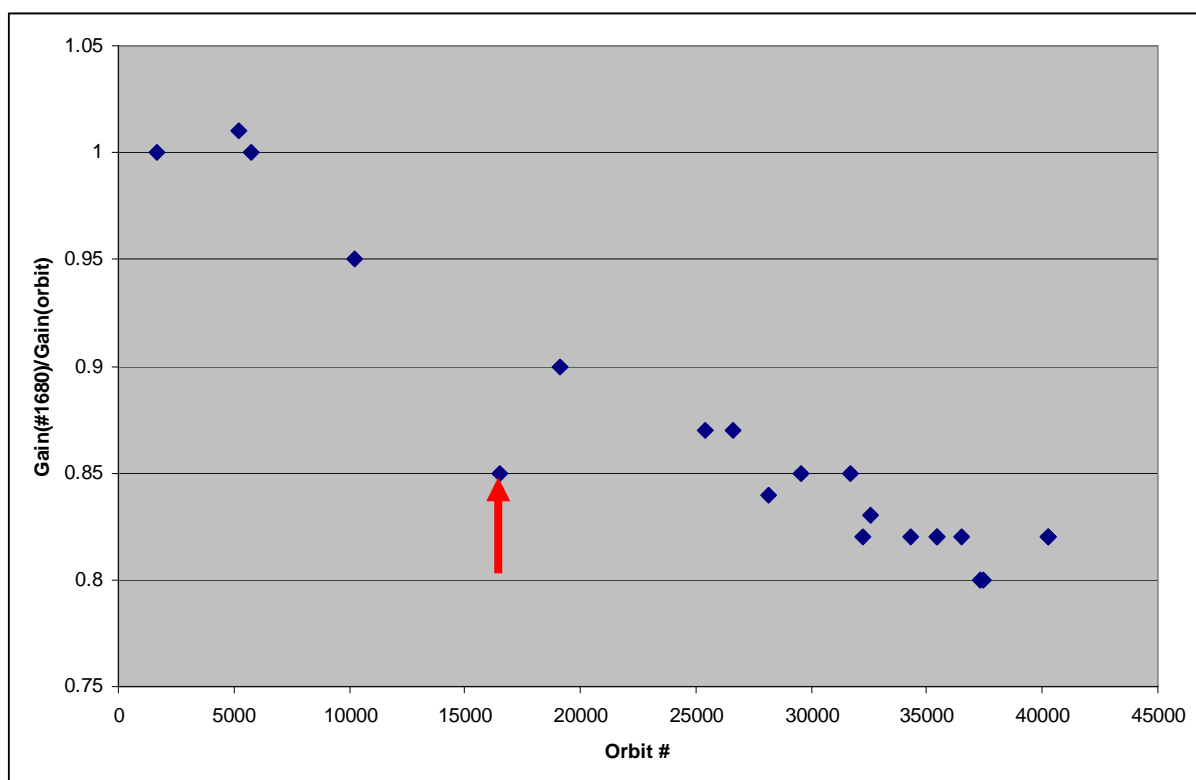


Figure 1. A2 channel detector degradation. The point at #16486 (red arrow) is that for the highest ice absorption. Since the spectral region without ice absorption is affected, the low value indicates scattering on a rough ice surface.

The most important information from the gainratio investigation for the following chapters is that the modulation efficiency has apparently not changed over the mission. The modulation efficiency is linked to the alignment of the interferometer and the beamsplitter optical quality. Furthermore the mirror quality is important but for the mid infrared this is usually no limitation. The modulation efficiency is 1 at 0 cm^{-1} and usually decreases with increasing wavenumber since the shorter wavelengths are more susceptible to wavefront distortion due to optical imperfections.

6 Fits of all available IF4/IF16 sequences

The procedure described in [RD2] was found to have a small bug which was fixed for the new method (see next chapter). Four parameters per detector ("BOMEM parameters") which are used in the level 1 processing were derived from DCnlin values instead of ADCmaxmin values.

In total five IF4/IF16 pairs were available throughout the mission. Figure 2 shows the zero and second order artifacts which are minimised by fitting the detector curve. Typically, beside a DS and a CBB interferogram, 9 scene interferograms for different tangent altitudes were entered into the fit. The following list gives an example taken from orbit 10173. The given tangent altitudes are simply calculated from the pointing angle and thus include an offset as well as a scalar with respect to the true tangent height. For all IF16 fitted always the lowest available tangent height (here 18.8 km) serves as reference for selecting the other ones (same tangent height steps).

R_EXT_0711-igm-B2.1_IF16_RAW_DS_0_	
R_EXT_0713-igm-A1.1_IF16_RAW_CBB_0_	
R_EXT_0716-igm-A1.16_IF16_RAW_SCE_0_	18.8 km
R_EXT_0719-igm-A1.9_IF16_RAW_SCE_0_	38.9 km
R_EXT_0719-igm-A1.11_IF16_RAW_SCE_0_	32.9 km
R_EXT_0719-igm-A1.13_IF16_RAW_SCE_0_	27.0 km
R_EXT_0719-igm-A1.15_IF16_RAW_SCE_0_	21.3 km
R_EXT_0716-igm-A1.8_IF16_RAW_SCE_0_	42.1 km
R_EXT_0716-igm-A1.10_IF16_RAW_SCE_0_	36.1 km
R_EXT_0716-igm-A1.12_IF16_RAW_SCE_0_	30.2 km
R_EXT_0716-igm-A1.14_IF16_RAW_SCE_0_	24.3 km

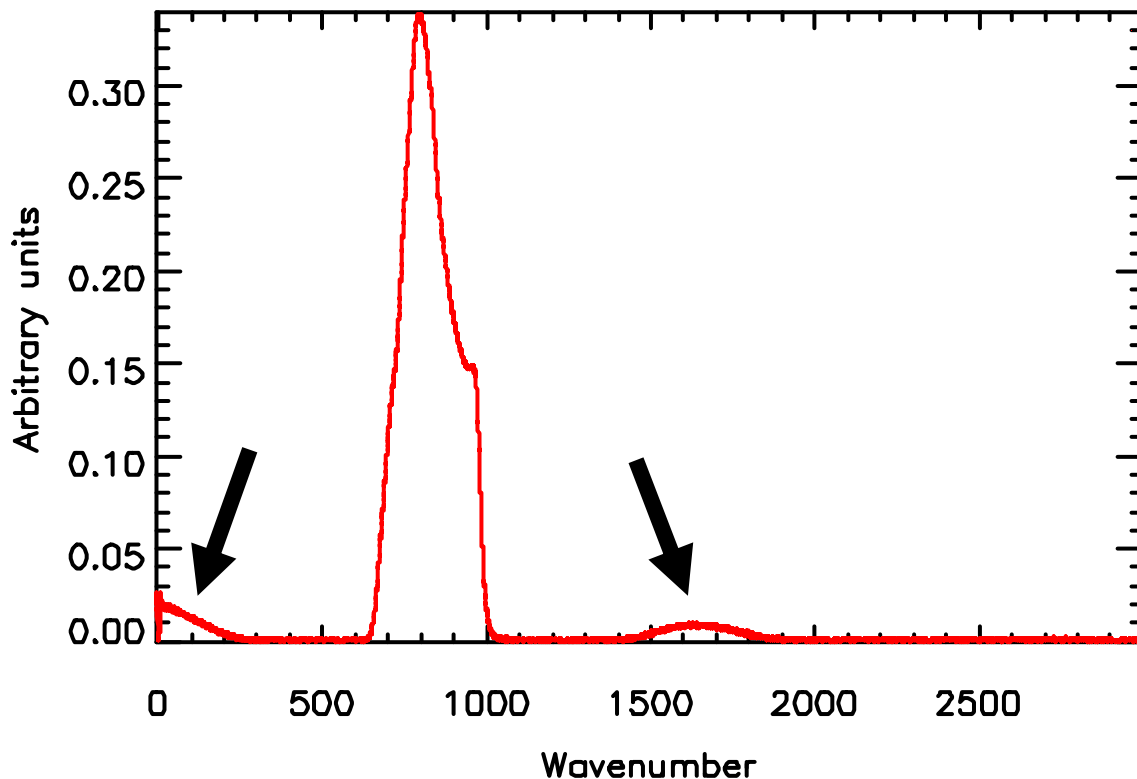


Figure 2. Example of out-of-band artifacts in A1 CBB spectrum.

Gain ratios are calculated from non-linearity corrected gains taking into account the non-linearity correction factors (details see [RD1] and [RD2]). These non-linear gain ratios are ratioed against that for the lowest CBB temperature. An example of these ratios for all channels and sweep directions for the most recent IF4 sequence is given in Table 2. The ratios increase with CBB temperature, are largest for A2 and smallest for B2.

Table 2. Example for gainratios.

Orbit	forw/rev	T(CBB)/K	Gainratios vs lowest T(CBB)			
			A1	A2	B1	B2
40320	0	230.544	1.0000	1.0000	1.0000	1.0000
40320	1	230.544	1.0000	1.0000	1.0000	1.0000
40283	0	243.636	1.0297	1.0466	1.0279	1.0160
40283	1	243.636	1.0299	1.0467	1.0286	1.0168
40357	0	249.654	1.0536	1.0825	1.0475	1.0422
40357	1	249.654	1.0521	1.0853	1.0444	1.0393
40375	0	250.376	1.0609	1.0941	1.0551	1.0480
40375	1	250.376	1.0596	1.0985	1.0518	1.0453

The fit yields the desired BOMEM parameters as well as the modulation efficiency.

Table 3. Modulation efficiencies.

Orbit	A1 forw	A1 rev	A2 forw	A2 rev	B1 forw	B1 rev	B2 forw	B2 rev
1680	0.924	0.930	0.862		0.817	0.843	0.824	
5764	0.934	0.929	0.876	0.871	0.815	0.830	1.157	1.250
10173	0.910	0.932	0.845	0.831	0.903	0.958	0.645	0.676
29538	0.828	0.837	0.771	0.751	0.751	0.765	0.442	0.480
40274	0.860	0.868	0.796	0.785	0.741	0.809	0.440	0.506

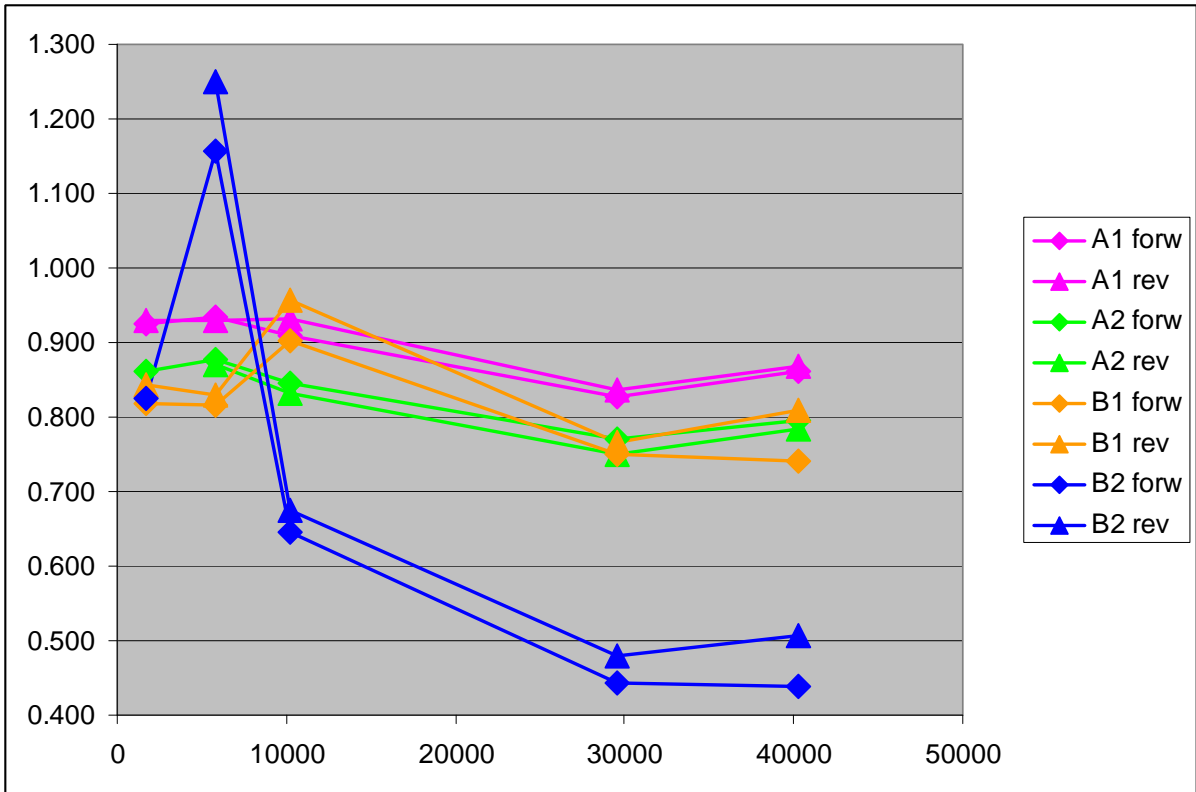


Figure 3. Modulation efficiencies vs. orbit number.

Table 3 summarises the modulation efficiencies for all channels, orbits, and forward/reverse. A graphical representation is given in Figure 3. The modulation efficiencies should remain unchanged during the mission since no optical degradation has taken place as can be derived from the unchanged channel D gainratios (see "Gainratio investigation").

The modulation efficiencies of channels A1, A2, B1 show a scatter of 10% while B2 scatter is very large. Since the B2 detector has the smaller non-linearity the information content on the modulation efficiency is rather low. There seems to be a downward trend vs. orbit number. However, it should be noted that the last two orbits were measured in reduced and the first three in full resolution mode and systematic errors may be influenced differently. The forward reverse differences are rather small indicating that statistical errors are not dominating the error budget seen in the differences.

Since the modulation efficiency is 1 at 0 cm^{-1} and decreases with wavenumber a quadratic dependence was assumed. Since forward and reverse data do not differ much and furthermore a complete data set was available only for forward direction further data reduction was carried out with forward modulation efficiencies only. The modulation efficiencies were fitted with a quadratic polynomial fixed to 1 at 0 cm^{-1} . The fitted curve matches the measured data well.

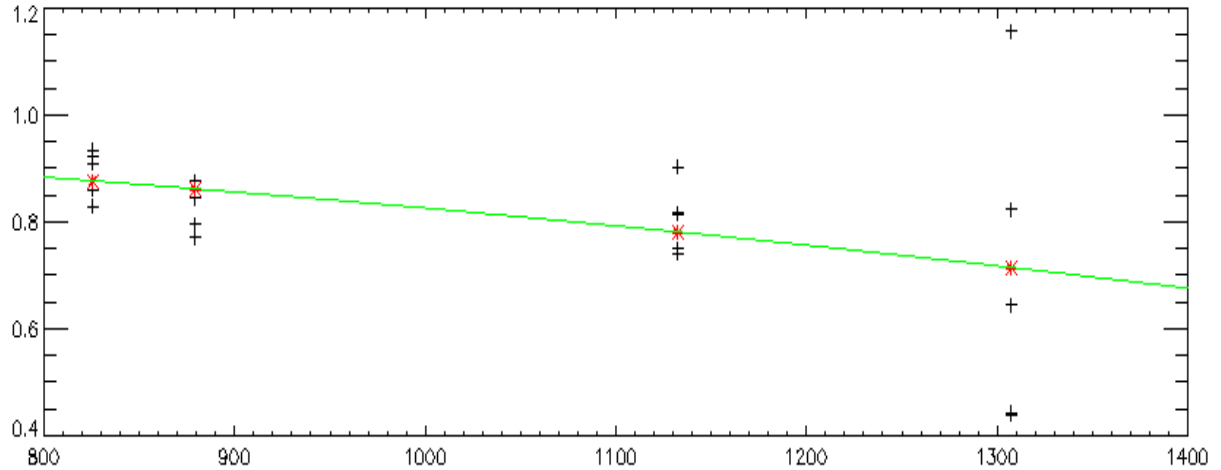


Figure 4. Fitted modulation efficiencies vs. center of gravity wavenumber of channels A1 to B2.

7 New method

It was always the goal to have a non-linearity characterisation method which only uses IF16 and which does not need the resource-consuming and thus very rare IF4 measurements. It was a coincidence triggered by the tests mentioned below to find such a method.

Tests revealed that the gainratios mainly influence the modulation efficiency while the out-of-band artifacts affect the non-linearity curve.

For example, changing the gain ratio for B2 by 1% (from 1.02549 to 1.01549) results in a change of the fitted modulation efficiency from 0.83 to 1.33, while the non-linearity correction factor is altered by less than 0.4%, which can be seen in Figure 3. This was confirmed by a similar test with the A1 channel. A modified code was written fitting the out-of-band data from the IF16 with the modulation efficiency fixed to the fitted values similar to those shown in Figure 4 but fitted with the modulation efficiency at 2200 cm⁻¹ fixed to 0.6 (see below). The method gave, as expected, a decent non-linearity characterisation.

As mentioned in the previous chapter a bug was found in the code: BOMEM parameters were fitted to DCnlin instead of ADCmaxmin. This affects the results presented in [RD2]. The correct procedure is to calculate the detector curve DCnlin vs. DClin, then to form derivatives of the inverse function dDClin/dDCnlin. The DCnlin values are then converted to ADCmaxmin, thus finally the derivatives are tabulated as function of ADCmaxmin. This is the input to the usual BOMEM parameter fit as described in [RD1].

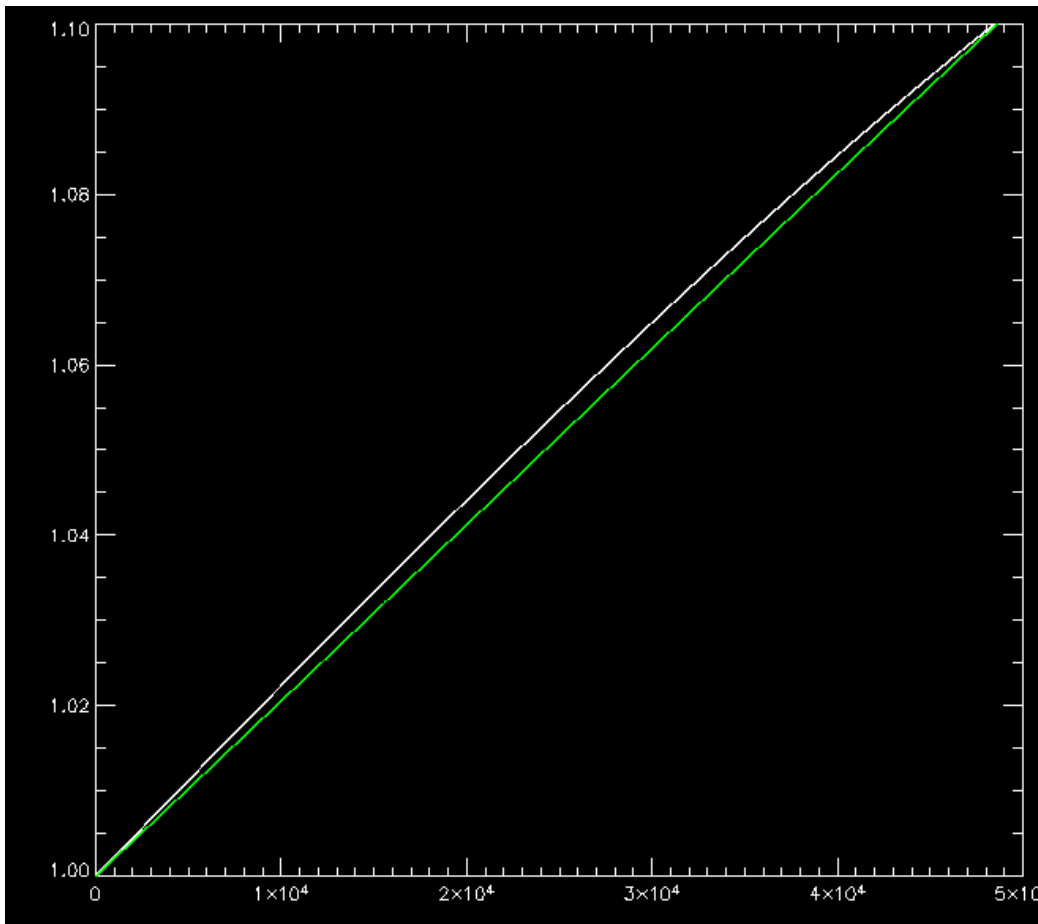


Figure 5. B2 Non-linearity correction factors vs. ADCmaxmin with and without a 1 % gainratio change.

As a first test the radiometric error introduced by an alteration of the modulation efficiency was investigated. Figure 5 does not directly show the radiometric error. After the mathematics for calculating radiometric differences when using different non-linearity correction curves have been updated, radiometric errors are much simpler than before (see below) since the radiance contrast error does only depend on the integral photon flux but not on the absolute value of the radiance contrast. When leaving out the outliers the difference between the fitted and measured modulation efficiencies is below 5% for channels A1, A2, and B1.

For B2 the modulation efficiency is somewhat extrapolated because of the large scatter in the measured values. Based on the polynomial the modulation efficiency at 2400 cm^{-1} has an unrealistic value of 0.1. Fixing the modulation efficiency at 2200 cm^{-1} to values between 0.5 and 0.8 the fitted modulation efficiency for B2 changes by not more than 5% and even less for the other channels. Figures 6 to 9 show the scalar radiance contrast change for a 10% modulation efficiency decrease. The error is largest at low integral photon flux, i.e. high tangent heights. Furthermore, the error is largest for A2 and smallest for B2. As stated before a 5% error bar on the modulation efficiency is realistic, thus, except the radiometric error is within 1.5% for A2 and within 1% for the other channels.

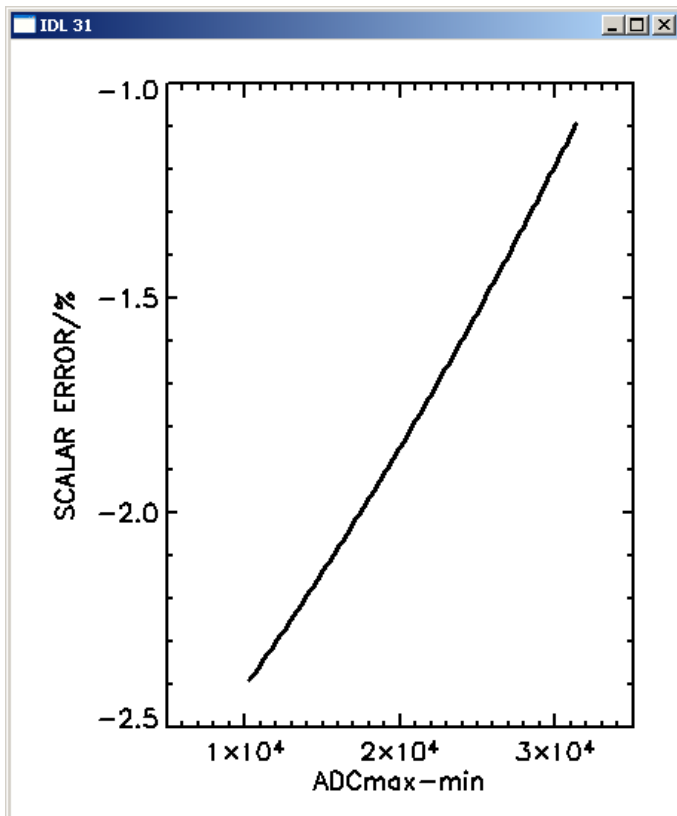


Figure 6. A1 rev 10230: Radiance contrast difference for non-linearity characterisation with 10% decreased modulation efficiency as function of ADCmaxmin.

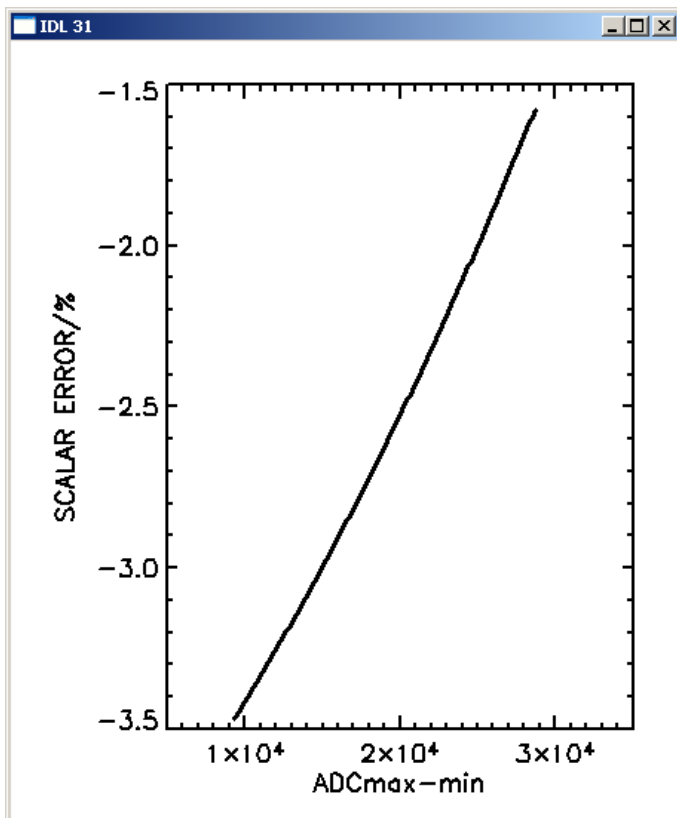


Figure 7. A2 rev 10230: Radiance contrast difference for non-linearity characterisation with 10% decreased modulation efficiency as function of ADCmaxmin.

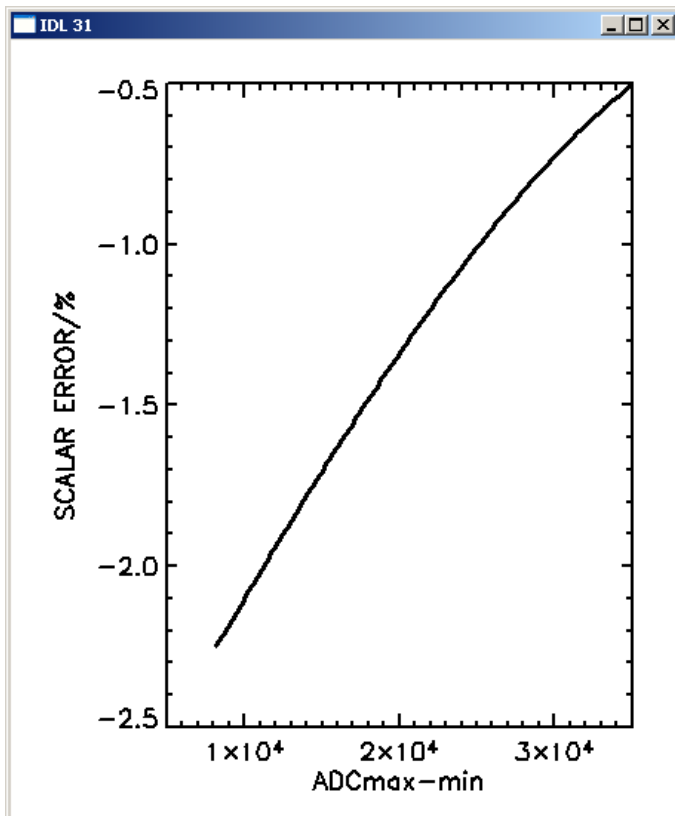


Figure 8. B1 rev 10230: Radiance contrast difference for non-linearity characterisation with 10% decreased modulation efficiency as function of ADCmaxmin.

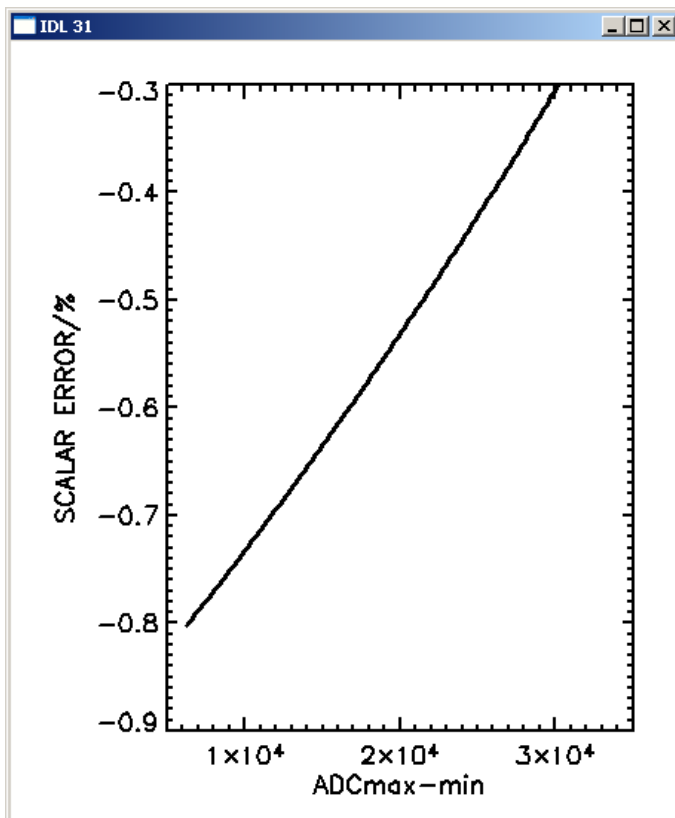


Figure 9. B2 rev 10230: Radiance contrast difference for non-linearity characterisation with 10% decreased modulation efficiency as function of ADCmaxmin.

8 Modifications and tests

Beside the removal of the gainratios there were more modifications done:

- Reduced phase resolution in modelled spectra for more symmetric residuals
- Improved selection of interferograms, DS added
- Improved convergence criterion
- Fits for various initial guesses and selection of best result
- Non-linearity characterisation for B1 and B2 with a quadratic term only
- No 0th order out-of-band artifact for B2
- Radiance contrast difference

Several tests were performed to confirm the validity of the method:

- Reproducibility
- Influence of which out-of-band artifacts are fitted
- Investigation of non-vanishing residuals for quadratic out-of-band artifacts

8.1 Reduced phase resolution in modelled spectra for more symmetric residuals

In the fit the interferograms are first truncated to 0.2 cm maximum optical path difference, linearised with the detector curve, Fourier-transformed and phase corrected with a phase calculated from the Hanning-apodised interferogram where the weight is zero for 0.02 cm optical path difference (old version: 0.1 cm). This helps to have noise residuals centered about zero. In the old version the higher phase resolution caused asymmetric noise residuals. Without phase correction the modulus would have only positive noise which may lead to wrong fit results with the fit trying to reach zero intensity.

8.2 Improved selection of interferograms, DS added

The DC zero method requires several measurements with different integral photon flux. The interferograms with different intensity help, first, to define the non-linearity curve and, second, to have good statistics for the ADC_{max} to DC_{lin} polynomial. In difference to the previous technote ([RD2]) better fit results are obtained when a DS measurement is included. A typical list of measurements can be found in "Fits of all available IF4/IF16 sequences".

8.3 Improved convergence criterion

It turned out that even when the IDL curvefit routine announces that a fit is converged further iterations lead to slightly different results. This may be caused by the regularisation but disabling the regularisation led to unstable fits. We thus modified the code to keep restarting the fit with the results of the previous fit as initial guess and only if 10 consecutive fits lead to changes of the quadratic non-linearity term by less than 0.01% the results were accepted.

8.4 Fits for various initial guesses and selection of best result

It turned out that the fit results even with the improved convergence criterion depend on the initial guess. To investigate this issue the dependence of χ^2 on the two parameters was

calculated. An example is shown in Figure 10. The χ^2 minimum is clearly visible at about -1.65]-0.365. The flat valley in the 10 o'clock direction indicates some correlation. A side minimum at higher χ^2 (red arrow) is located at in the blue line above the big valley. The trouble is that if the initial guess is at an unfortunate place the side minimum is reached. The reason for this behaviour may be that in contrast to standard least squares fitting experimental data with noise are involved in the model. Usually, the model is purely algebraic and thus practically noise free and the observed-calculated vector is then built linearly with the experimental data. The appearance of side minima was found to be very unpredictable and varied from fit to fit. It was found that typically within 7 different initial guesses of the quadratic parameter which are distributed $\pm 15\%$ about the expected result, at least two led to approximately the same smallest χ^2 . The problem was more pronounced where less non-linearity is present, which led to removal of the cubic term in the B1 and B2 channel fits.

8.5 Non-linearity characterisation for B1 and B2 with a quadratic term only

Stable fits with a cubic term for B2 were rare, for B1 the situation was better, but still the strong initial guess dependence was unsatisfactory. Thus, the third order term was omitted in fits for channels B1 and B2. In order to illustrate the error associated with this reduction Figures 11 and 12 show 2 examples for radiometric differences between fits with quadratic and quadratic + cubic terms. The differences show the same trend in both cases but are well within 0.5%. Certainly the reality is closer to the 2 parameter than the 1 parameter solution, but the small error is accepted with the benefit of stable fits.

8.6 No 0th order out-of-band artifact for B2

As shown later the results do not much depend on whether the 0th order + 2nd order artifacts are used together or only one of them. Of course more information is present when fitting both of them. In a very early stage of the analysis an intercomparison between B2 results from five different orbits indicated better consistency when leaving out the 0th order. This was never consolidated with all modifications and all orbits analysed. Nevertheless, the 0th order was removed from the B2 fit.

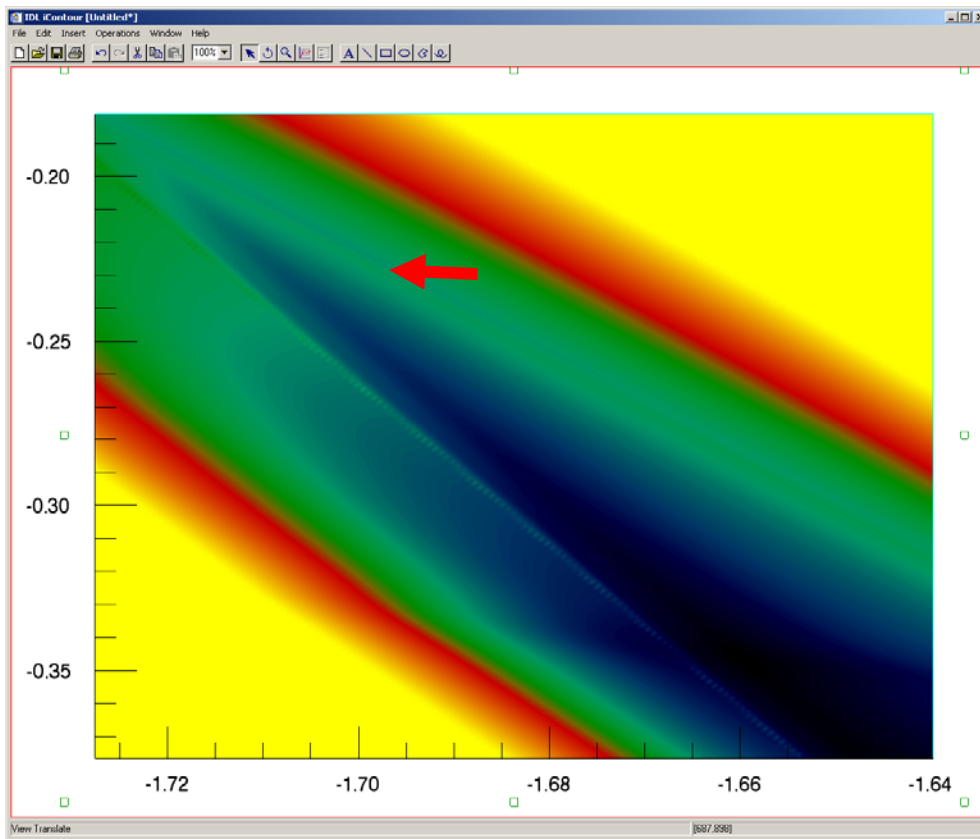


Figure 10. #16486 A1 forw. χ^2 vs quadratic (x-axis) and cubic (y-axis) non-linearity contributions, plot range 1% of χ^2 .

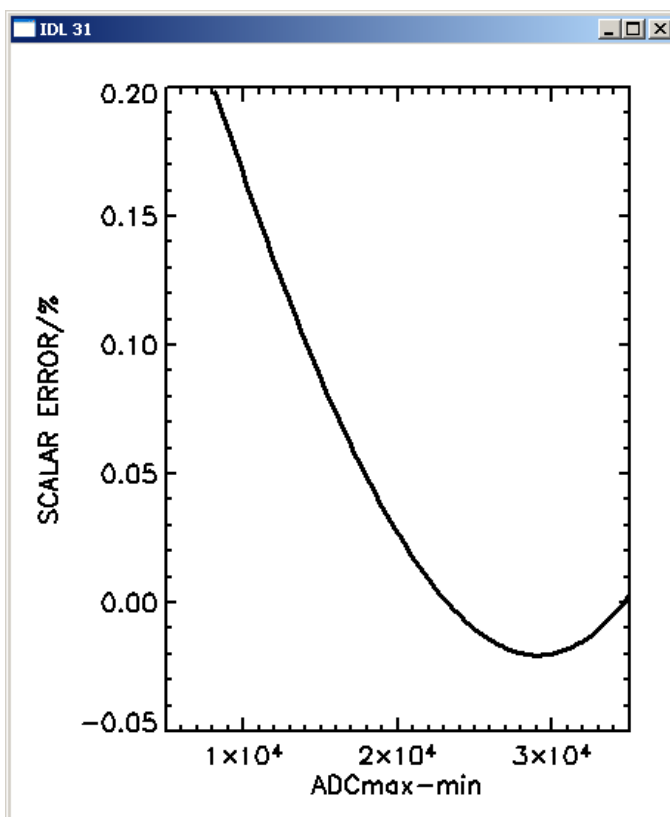


Figure 11. Orbit 1680, B1, forw. Radiance contrast difference for non-linearity characterisation with and without cubic coefficient in detector non-linearity curve.

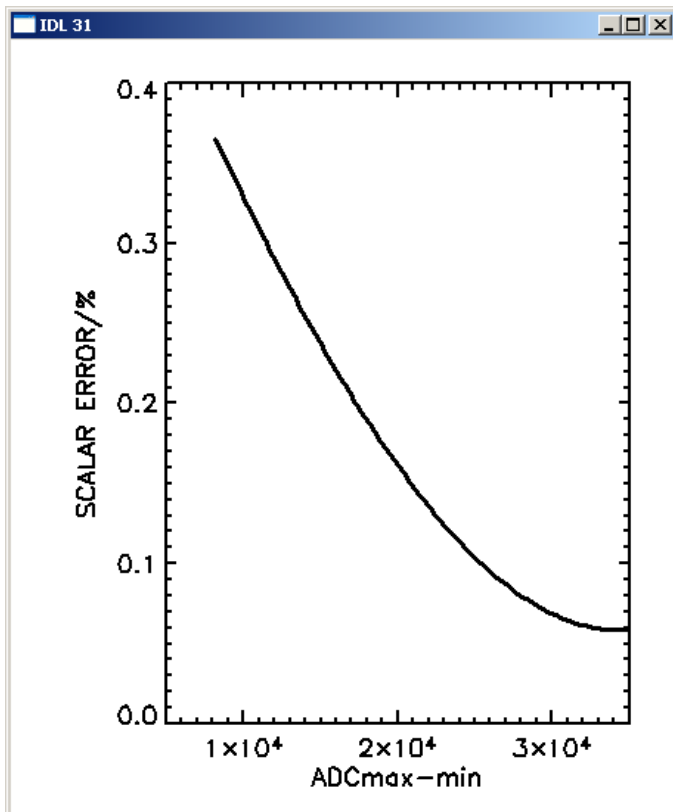


Figure 12. Orbit 40274, B1, forw. Radiance contrast difference for non-linearity characterisation with and without cubic coefficient in detector non-linearity curve.

8.7 Radiance contrast difference

In the old documentation radiometric differences caused by two different non-linearity correction curves were defined in terms of absolute radiance inputting the different set of BOMEM parameters (Percentage absolute radiance difference= $\Delta L/L$, ΔL =radiance difference for both parameter sets, L =absolute radiance). The percentage absolute radiance difference is dependent on the integral photon flux as well as the actual spectral photon flux. Usually the analysis of atmospheric radiance spectra is based on molecular lines which are located on a radiance background. The level 2 product error can be related to the line intensity which is a radiance contrast. Thus, the error characterisation of non-linearity is more convenient when expressed in terms of radiance contrast instead of absolute radiance. IDL code was developed to calculate percentage radiance contrast differences. Initially, the radiance error is calculated as function of integral and spectral photon flux. It is assumed that the spectral intensity of DS is 0.2, that of the CBB 1.0 and that the atmospheric spectral intensity is in between. From experimental spectra it was shown that this value is reasonable. Then a contrast difference is simply calculated by forming differences and the percentage difference by dividing by the radiance contrast: $(\Delta L_{\text{peak}} - \Delta L_{\text{base}})/(L_{\text{peak}} - L_{\text{base}})$. It turned out that the percentage contrast difference is neither depending on the radiance contrast magnitude nor on the baseline spectral intensity for the contrast. The only dependence is on the integral photon flux. The error can also be expressed as an offset error which is defined as radiance error of a horizontal baseline with all spectral points having the same spectral intensity.

8.8 Reproducibility

Figures 13 to 16 show radiometric differences for one example orbit when using a different set of interferograms. Most of the differences are within 0.5% where the largest difference for B2 is

linked to the smallest detector non-linearity and thus smallest amount of information. These results give an impression about the statistical errors.

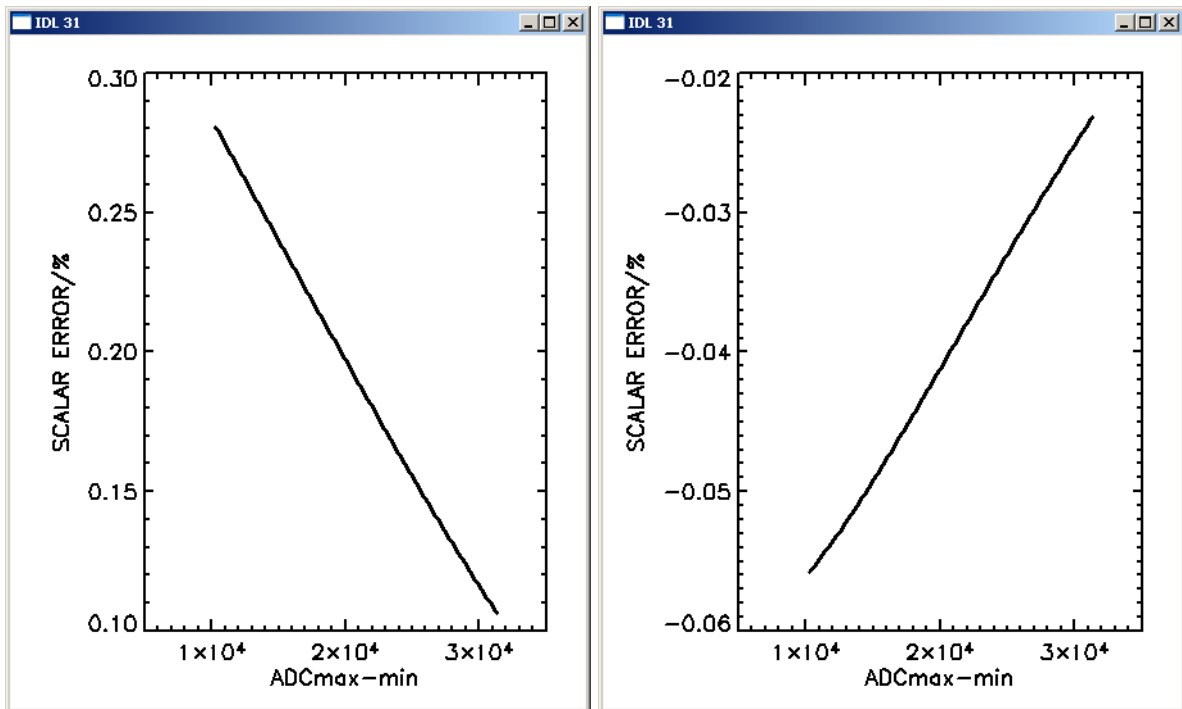


Figure 13. A1 forw(left), rev(right) #40274. Radiance contrast difference for non-linearity characterisation with different interferograms.

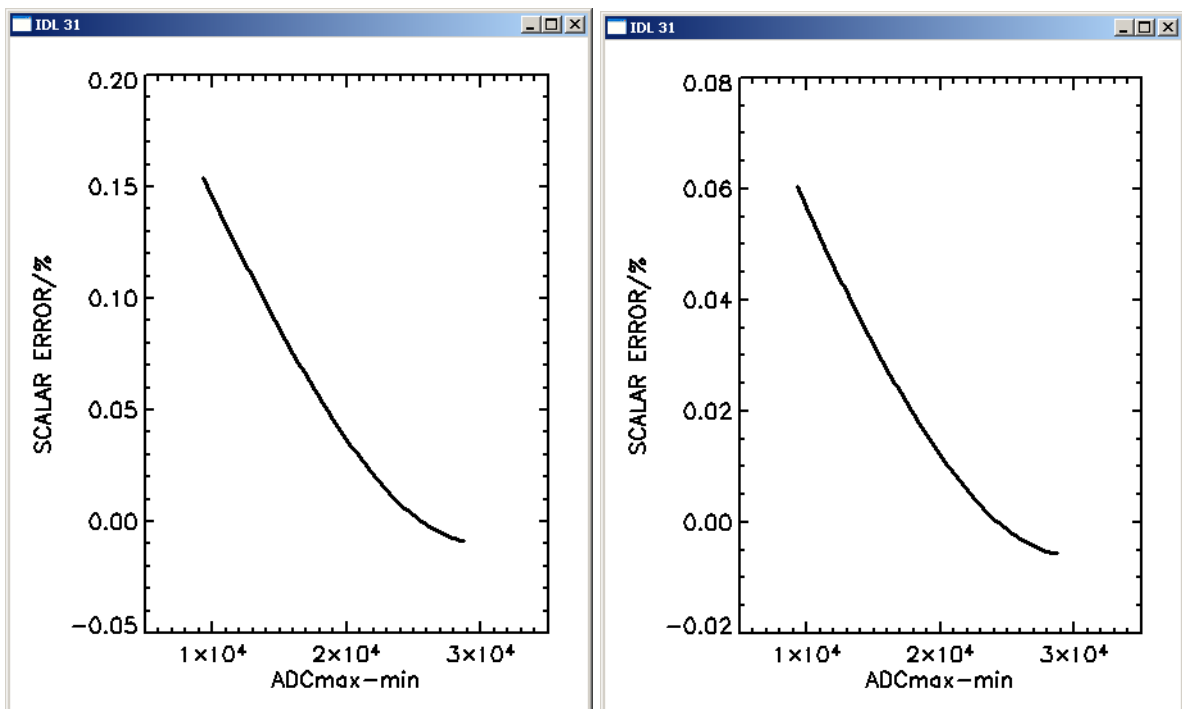


Figure 14. A2 forw(left), rev(right) #40274. Radiance contrast difference for non-linearity characterisation with different interferograms.

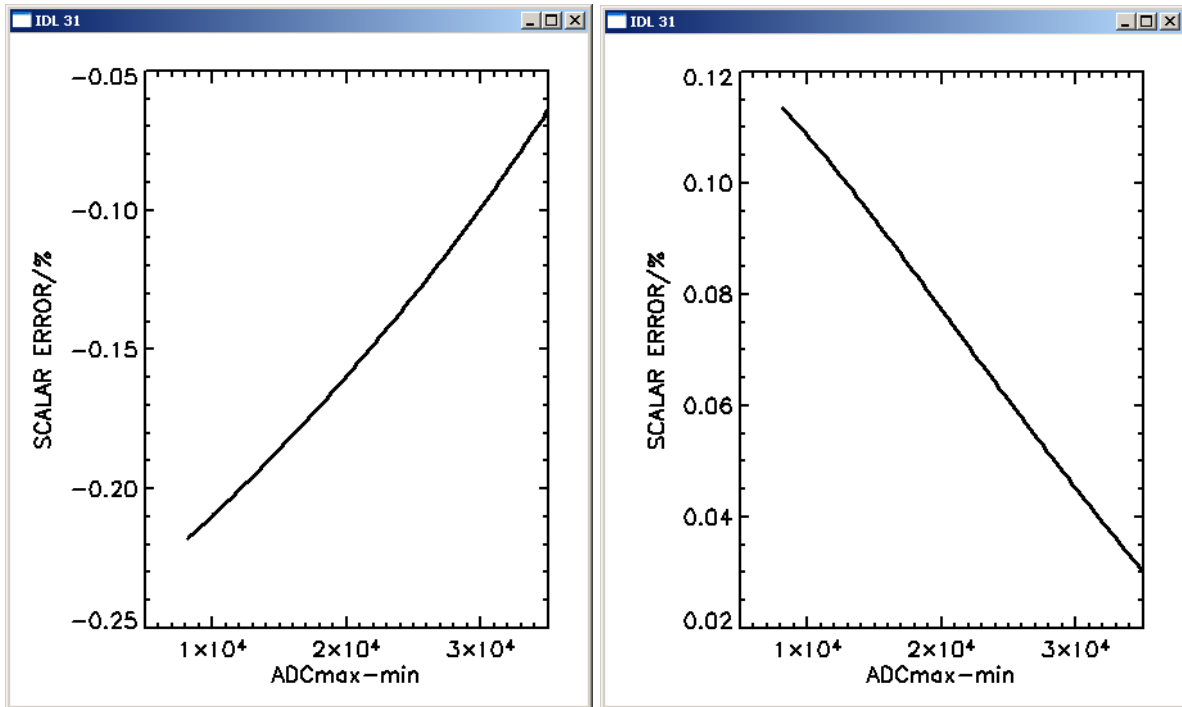


Figure 15. B1 forw(left), rev(right) #40274. Radiance contrast difference for non-linearity characterisation with different interferograms.

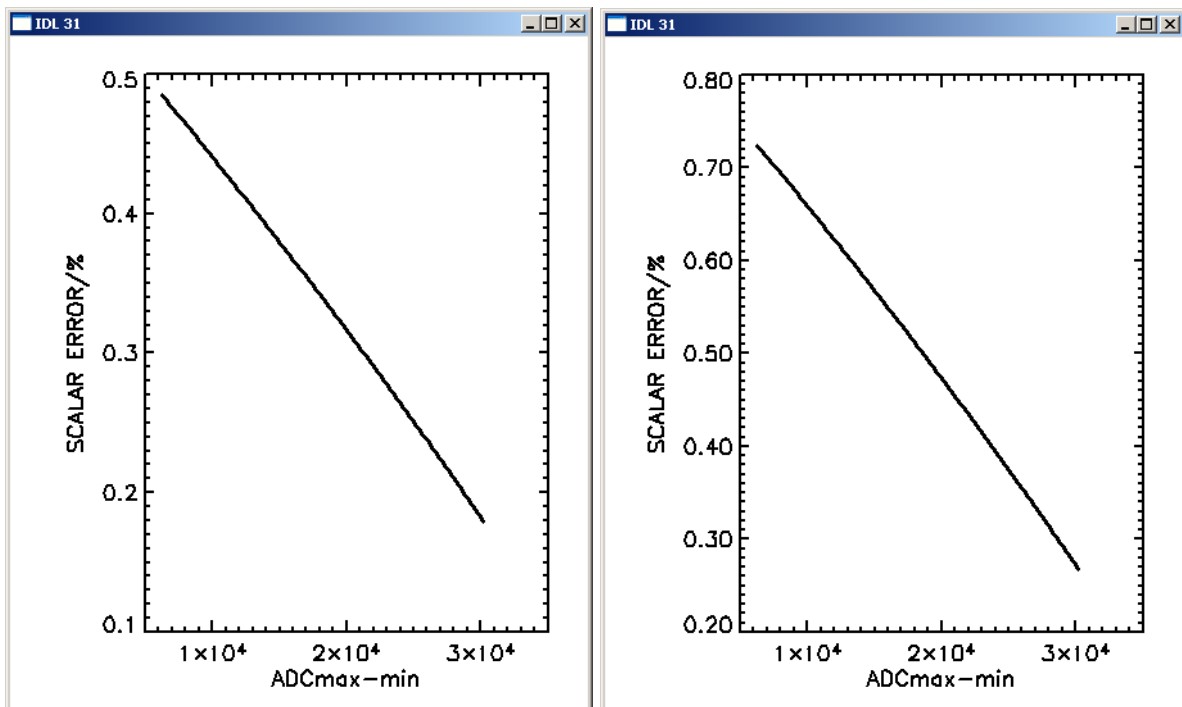


Figure 16. B2 forw(left), rev(right) #40274. Radiance contrast difference for non-linearity characterisation with different interferograms.

8.9 Dependence on out-of-band artifacts

There are three distinct spectral artifacts introduced by the non-linearity and removed to characterise the detector curve, the 0th, 2nd, and 3rd order artifact. While 0th is influenced by quadratic and cubic non-linearity the 2nd order artifact is influenced by the quadratic non-

linearity only, the 3rd by the cubic non-linearity. The 0th order artifact contains also 1/f noise and all kinds of mechanical and electronic perturbations. The 3rd order artifact is very small and thus, information content is also very small but still included in the analysis. Figure 17 shows the largest (A2, CBB) out-of-band contribution before and after the fit as well as the ranges used in the fitting. Due to the 1/f noise the 0th order artifact was only used above 150 cm⁻¹. A screenshot of the fit is shown in Figure 18. The out-of-band spectral regions indicated as bars in Figure 17 are concatenated for all interferograms to form the plot in Figure 18. As in Figure 17 the spectrum before and after non-linearity correction is shown.

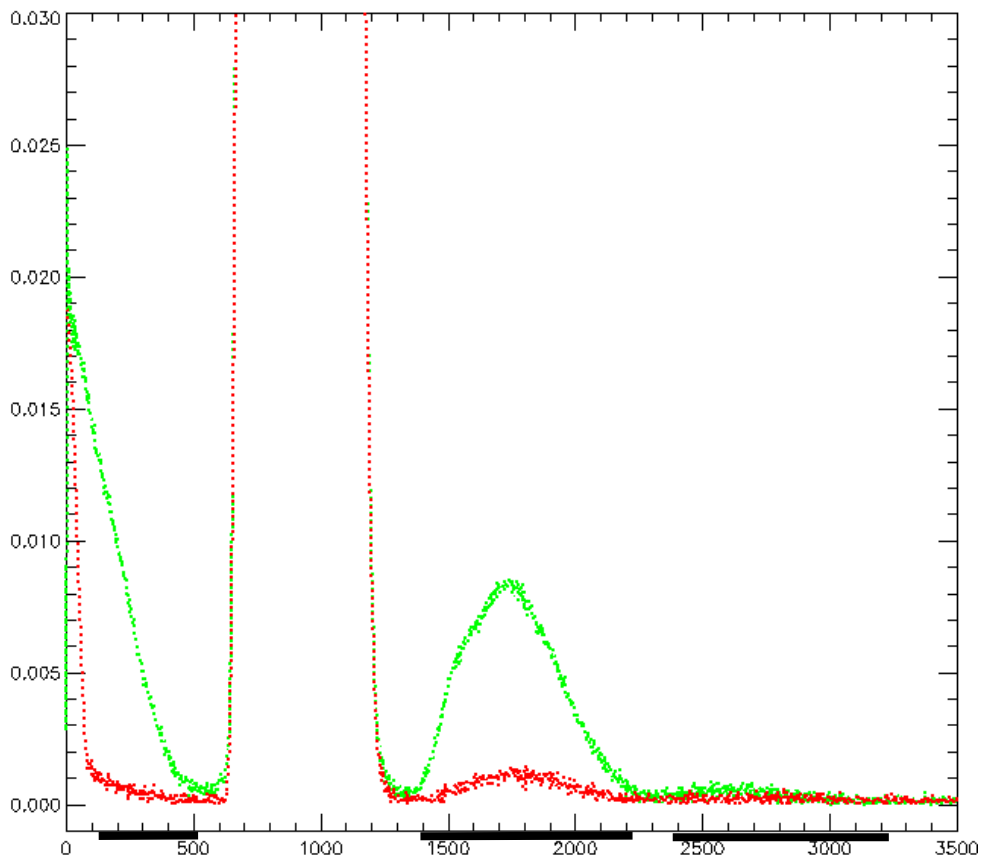


Figure 17. CBB A2. Green: original spectrum, red: non-linearity corrected spectrum, black: ranges used in non-linearity characterisation fit.

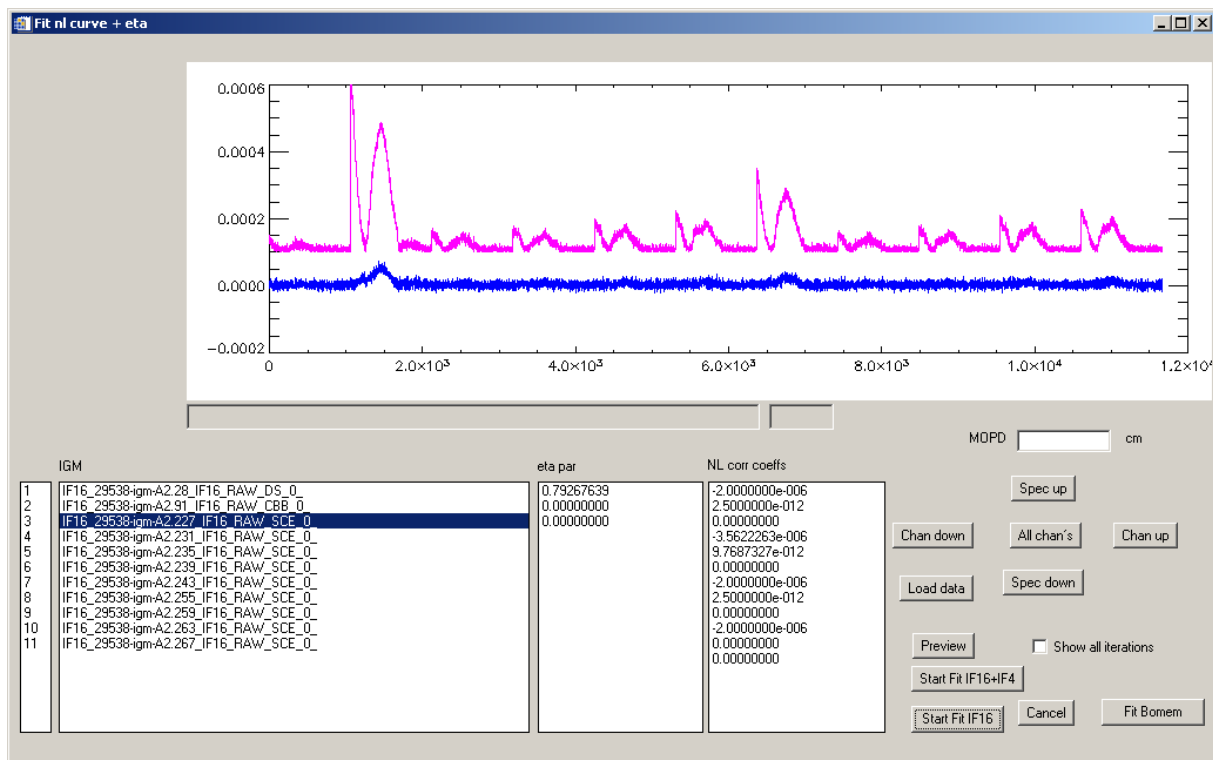


Figure 18. Screenshot of non-linearity fit. Purple: concatenated out-of-band artifacts for all measurements used in the fit. Blue: residual out-of-band artifacts after non-linearity fit. Below the graph is a list of the interferograms entered into the fit.

In principle the 0th and 2nd order artifacts should give the same results. There are non-zero residuals more pronounced for the 2nd order artifact which are discussed in the section “Investigation of non-vanishing residuals for quadratic out-of-band artifacts”.

The effect of the selection of artifacts on the fit results was investigated for an example orbit (10230). Extra fits were done for the 0th order artifact only and the combination 2nd and 3rd order. Radiometric differences between the two cases and between the standard fit with all orders and the combination 2nd and 3rd order are shown in Figures 19 to 21 for channels A1 to B1. For B2 the 0th order artifact is omitted in the fit (see above). An example for B2 in Figure 22 shows small radiometric differences between fits with and without 0th order artifact. The radiometric differences between 0th order and 2nd+3rd order results are up to 1.3%. With respect to the nominal case with all orders the differences are up to about 0.5%. To investigate if the large A2 differences are common, a second orbit was investigated shown in Figure 23. The differences are much smaller. From the few cases investigated the statistics is too small for a defined conclusion about a systematic influence of a specific order on the fit results. Anyhow, the differences found so far are moderate.

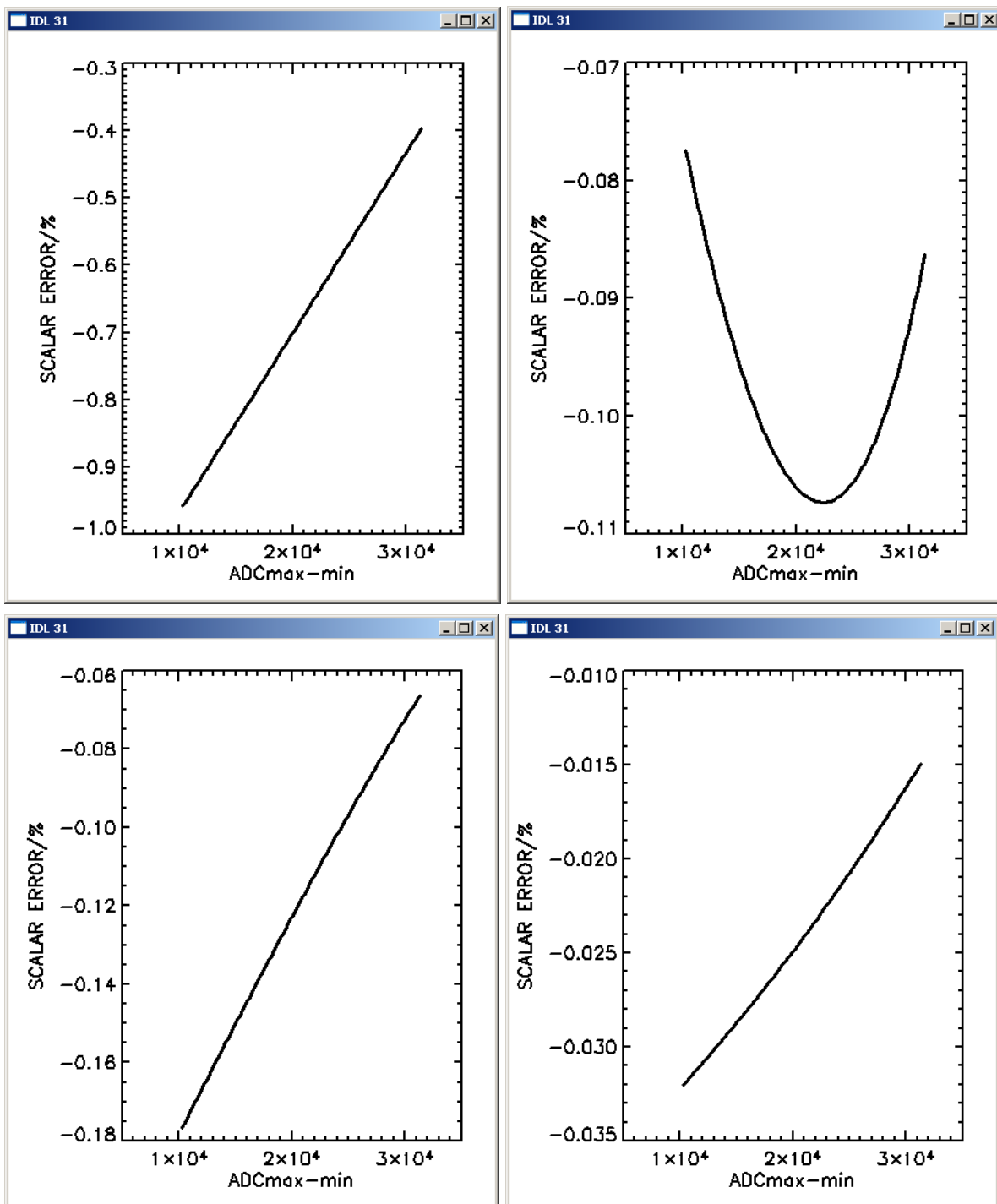


Figure 19. A1 forw(left), rev(right) #10230. Radiance contrast difference for non-linearity characterisation with 0th order out-of-band artifacts only and 2nd order out-of-band artifacts only (top) and with 0th and 2nd order out-of-band artifacts and 2nd order out-of-band artifacts only (bottom).

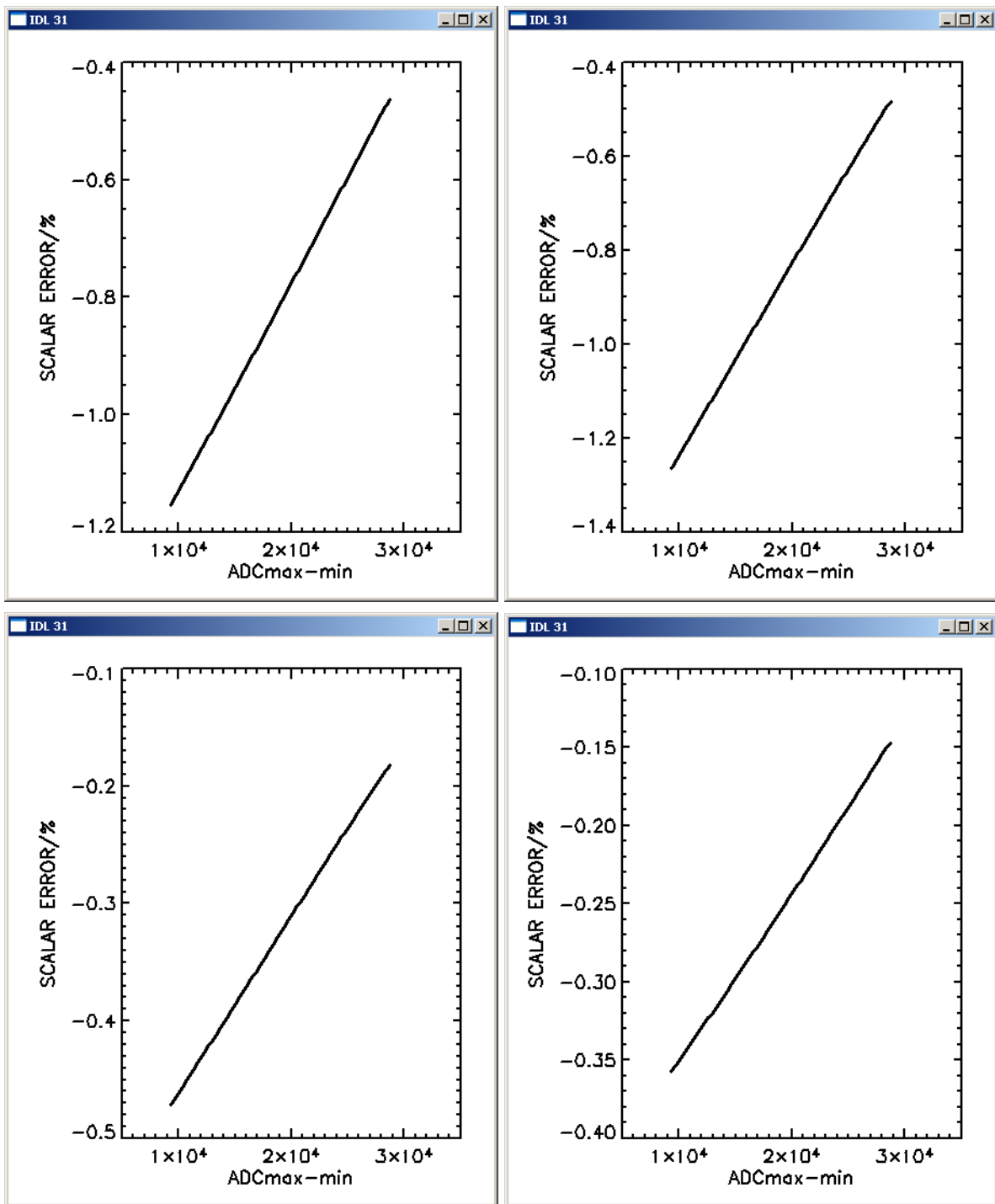


Figure 20. A2 forw(left), rev(right) #10230. Radiance contrast difference for non-linearity characterisation with 0th order out-of-band artifacts only and 2nd order out-of-band artifacts only (top) and with 0th and 2nd order out-of-band artifacts and 2nd order out-of-band artifacts only (bottom).

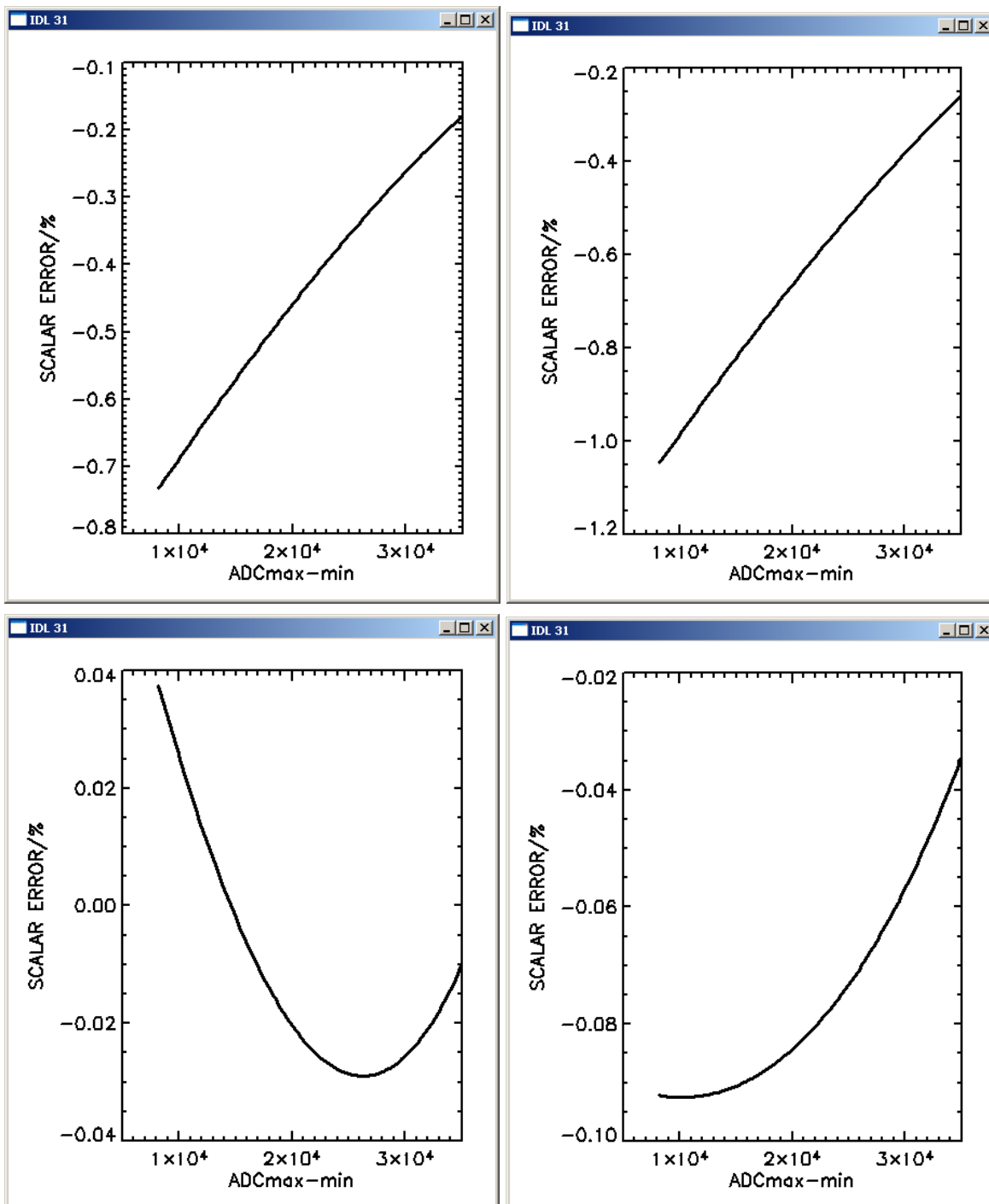


Figure 21. B1 forw(left), rev(right) #10230. Radiance contrast difference for non-linearity characterisation with 0th order out-of-band artifacts only and 2nd order out-of-band artifacts only (top) and with 0th and 2nd order out-of-band artifacts and 2nd order out-of-band artifacts only (bottom).

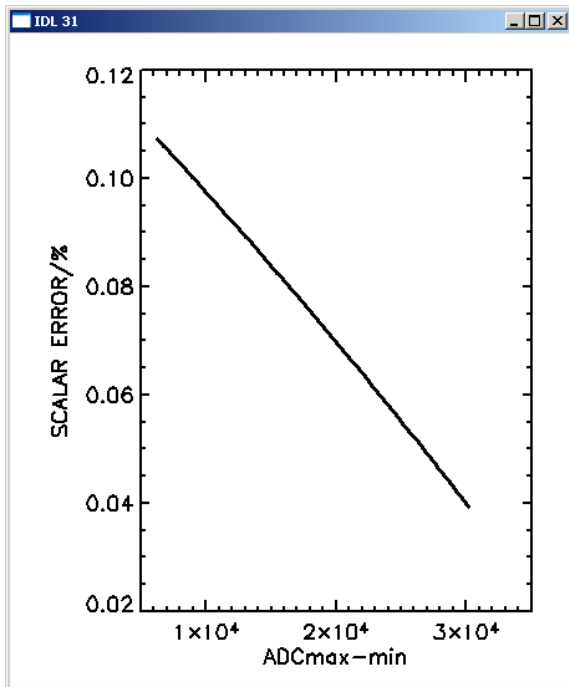


Figure 22. Orbit 1680, B2, forw. Radiance contrast difference for non-linearity characterisation fitted with and without 0th order artifact, both with only quadratic coefficient in detector non-linearity curve.

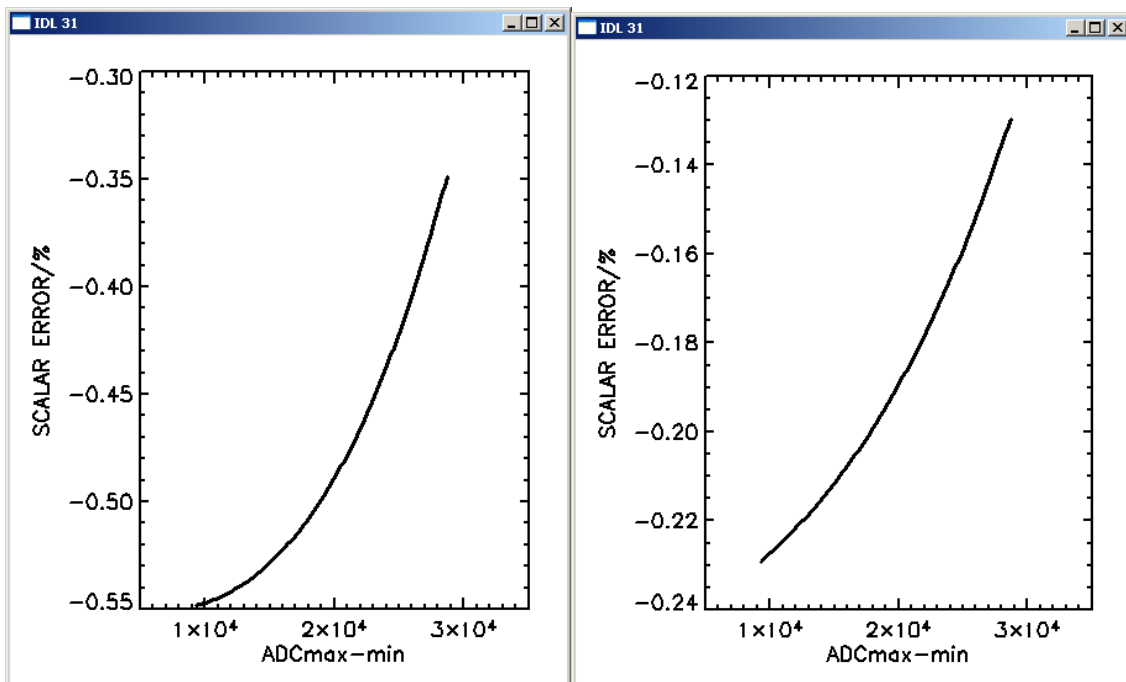


Figure 23. A2 forward 40274. Radiance contrast difference for non-linearity characterisation with 0th order out-of-band artifacts only and 2nd order out-of-band artifacts only (left) and with 0th and 2nd order out-of-band artifacts and 2nd order out-of-band artifacts only (right).

8.10 Investigation of non-vanishing residuals for quadratic out-of-band artifacts

Figure 18 shows distinct residuals for the 2nd order out-of-band artifact. It is surprising that the artifact did not disappear when fitting the 2nd order region alone, even when fitting only a single measurement. Synthetic data revealed that any out-of-band feature can be fitted to the noise level. Thus, the phase of the residual artifact was investigated. Figure 24 shows a plot of the phase with and without non-linearity correction and the difference. The phase of the residual has a 90° difference to the original 2nd order artifact, which of course dominates the phase since it is about 5 times stronger, as can be seen in Figure 18. The physical nature is unclear. Anyhow, it is not disturbing the non-linearity fitting.

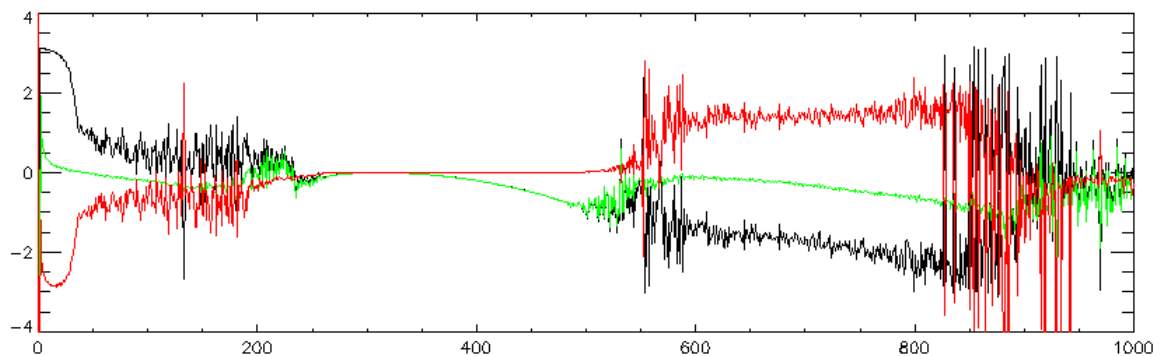


Figure 24. A2 CBB. Green: Phase for the original spectrum. Black: Phase of the non-linearity corrected spectrum. Red: Difference. The region 600 to 800 points corresponds to the 2nd order artifact region (see also Figure 15).

9 Calculation of effect of ice and instrument temperature

In [RD5] the ice and instrument temperature influence on non-linearity was quantified. However, at this time the radiance contrast difference was not introduced yet. Thus, with inputs from [RD5] radiometric differences for 67% peak ice absorption were calculated. It should be emphasised that these calculations are based on not scattering ice surfaces and the noise model as described in RD3. Figure 25 shows the results which are largest for channel A2. Figure 26 shows the effect of 10 K temperature decrease. Again, the largest effect was found for channel A2.

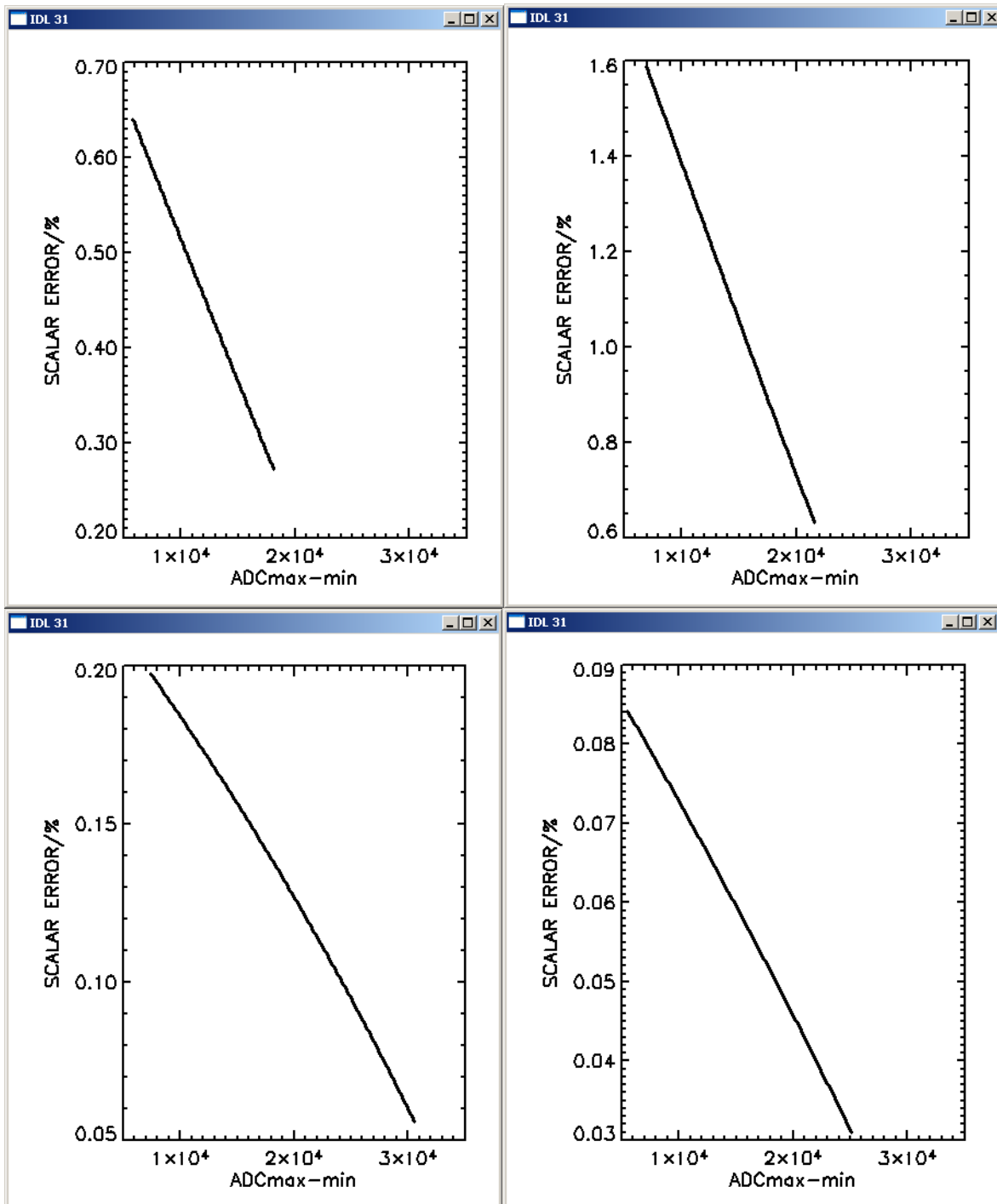


Figure 25. Channel A1 to B2 (left to right, top to bottom). Radiometric differences caused by 67% ice peak absorption.

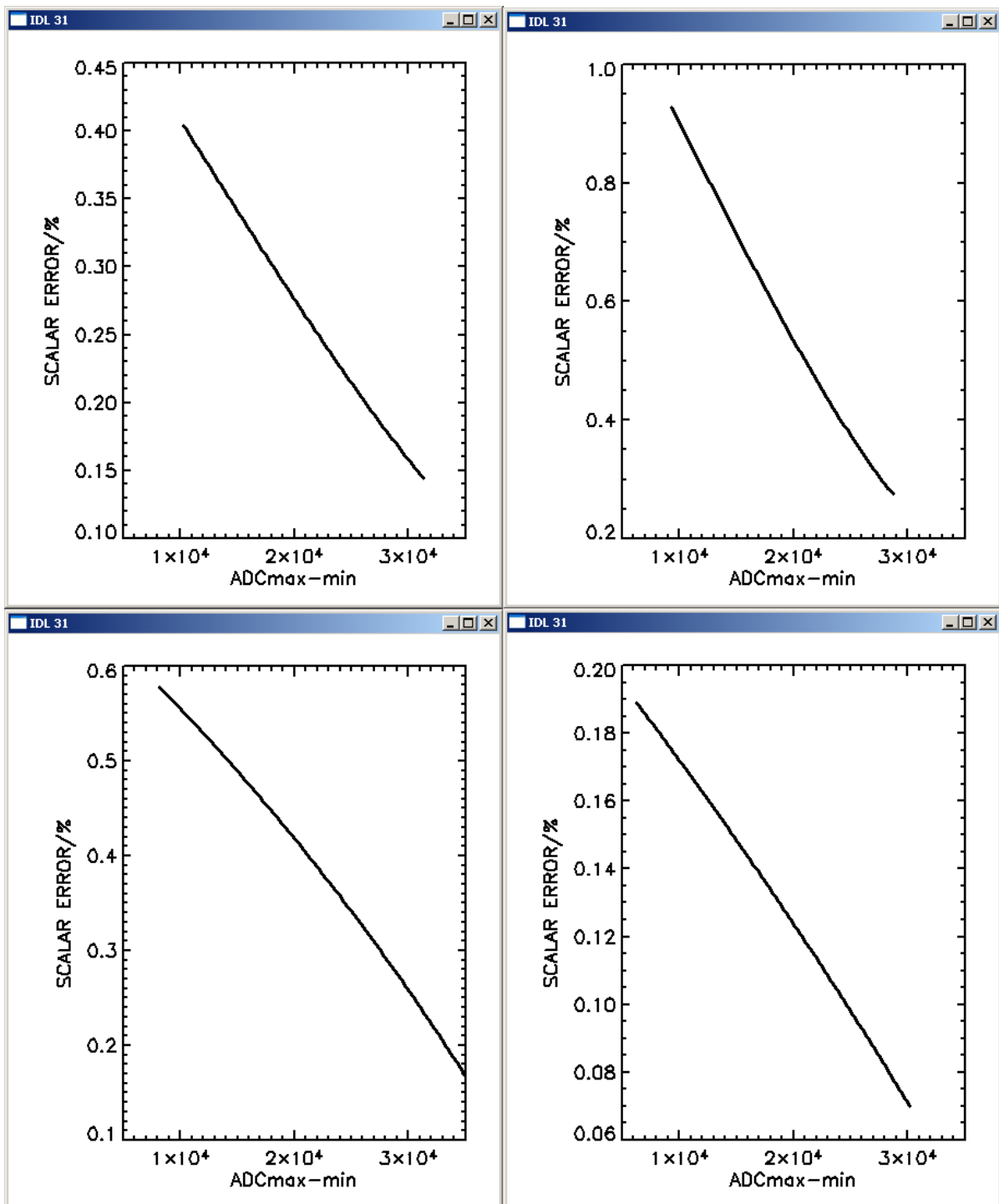


Figure 26. Channel A1 to B2 (left to right, top to bottom). Radiometric differences caused by 10K instrument temperature decrease.

10 Results of single orbit fits

Fits of all available IF16 orbits were performed. In the final version of the fitting tool all IF16 data are fitted automatically which takes a few days. The fit output is compiled in a text file. In order to investigate the variation of the non-linearity among these orbits maximum radiometric differences with respect to the earliest orbit (#1680) were tabulated. Usually, the maximum difference occurs for smallest integral radiance as can be seen in the many plots showing

radiometric differences (for example see Figure 23). The respective values given for the four channels, forward and reverse, can be found in Tables 4a and b. The differences are affected by reproducibility, but also systematic influences such as ice contamination and instrument temperature. It should be noted that the radiometric differences are based on ADCmaxmin values. In case the sampling of the interferogram changes between respective and reference orbit a radiometric difference occurs. All differences are smaller than 4%. Forward/reverse differences give information about the consistency and show outliers. Most of the differences are well within 0.5% which is in line with the statistical uncertainty (see section "Reproducibility"). In case of orbit #35406 A1 forward the minimum χ^2 was not the right solution and was thus replaced by the correct one (solution occurring for more initial guesses). For orbit #16486 with heavy ice contamination unfortunately the number of available scene measurements was limited influencing the quality of the fit, especially for A1. The radiometric differences are clearly correlated with orbit number as can be seen in Figures 27 to 30. The aging of the detectors makes them less sensitive and thus more linear. The effect of ice can also be seen. The information on ice contamination was obtained from gainratios of channel A2 from the peak of the ice absorption and the unperturbed high wavenumber end of the A2 spectrum. The ice absorption for orbit i vs. #1680 is given by $[1-G_{1680}(\text{peak})/G_i(\text{peak}) * G_i(\text{high})/G_{1680}(\text{high})]$. Except for channel A1 forward Tables 4a and b show significant larger differences for orbit #16486 with 53% ice contamination. Given the strong effect of aging it is hard to dig out the temperature correlation which is predicted to be rather small. The instrument temperatures are also given in the Tables and are taken from level 1a housekeeping data.

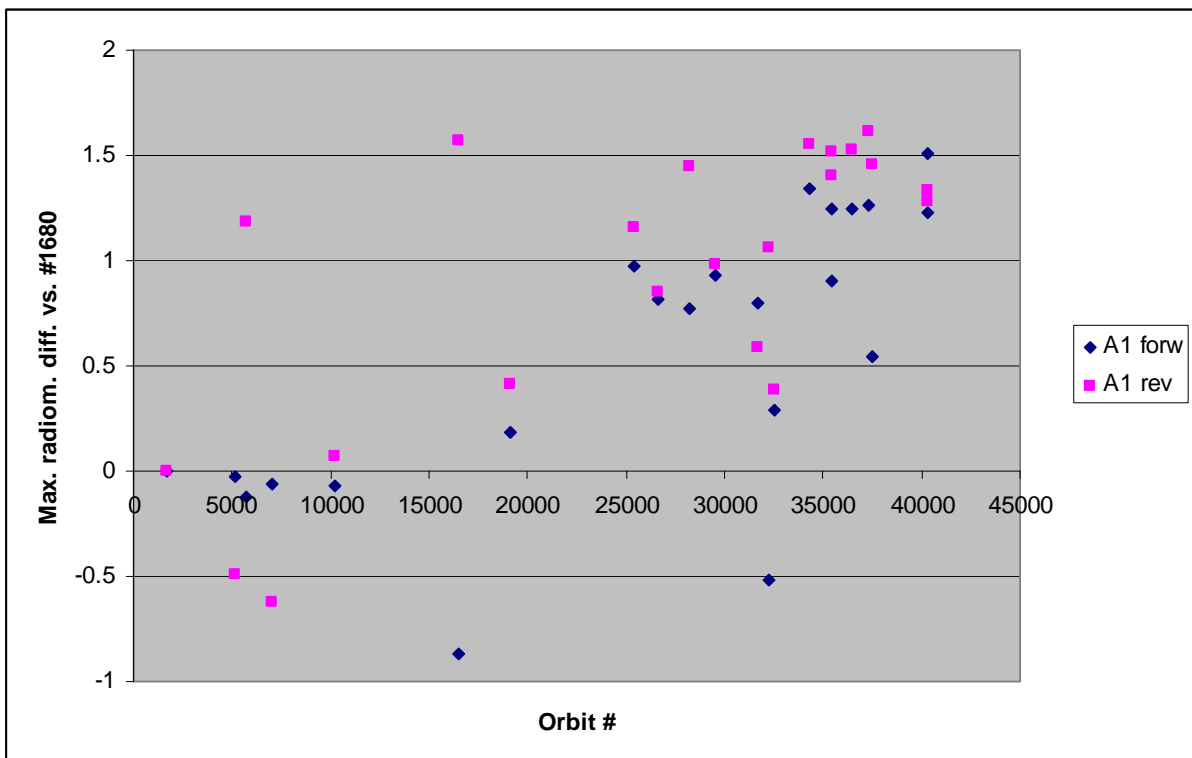


Figure 27. A1. Maximum radiometric differences to orbit #1680 vs. orbit number.

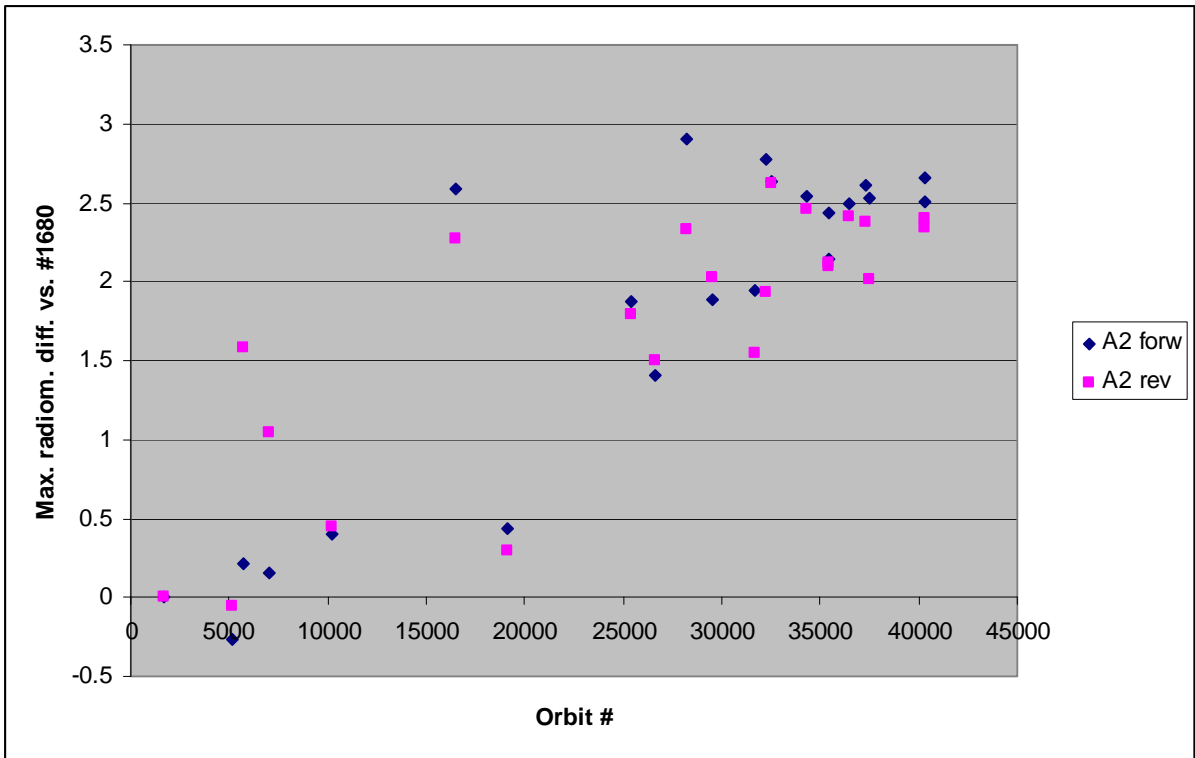


Figure 28. A2. Maximum radiometric differences to orbit #1680 vs. orbit number.

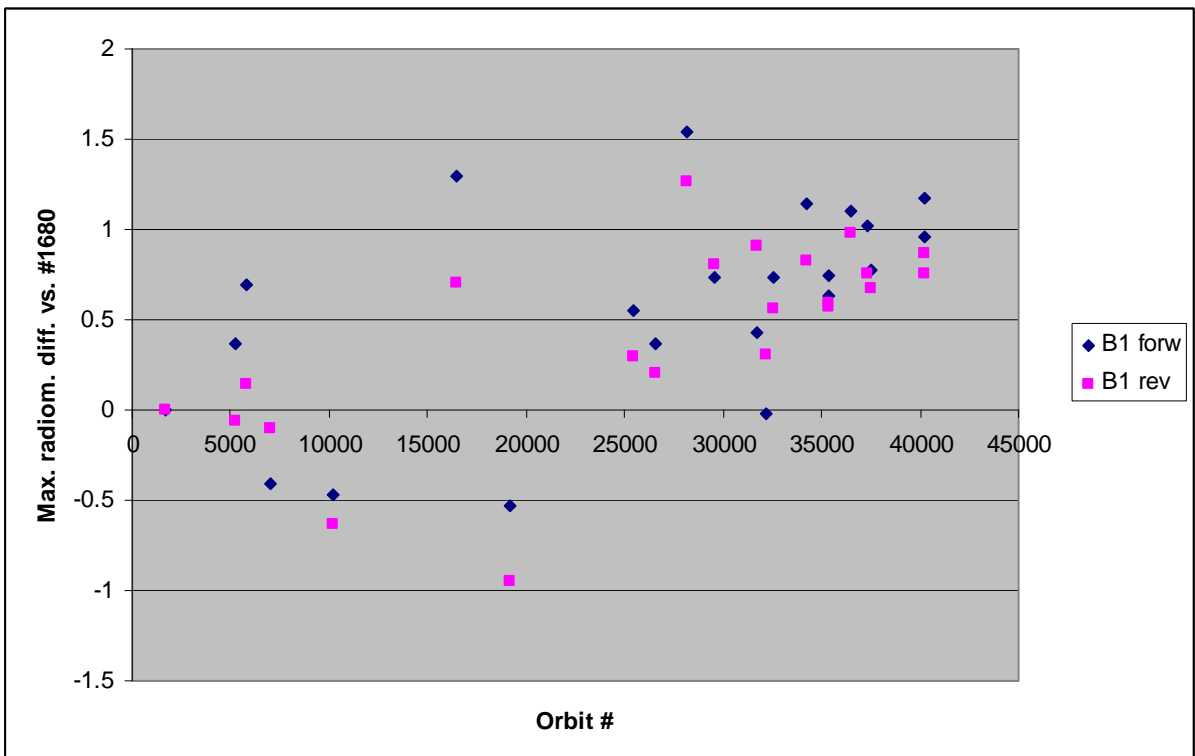


Figure 29. B1. Maximum radiometric differences to orbit #1680 vs. orbit number.

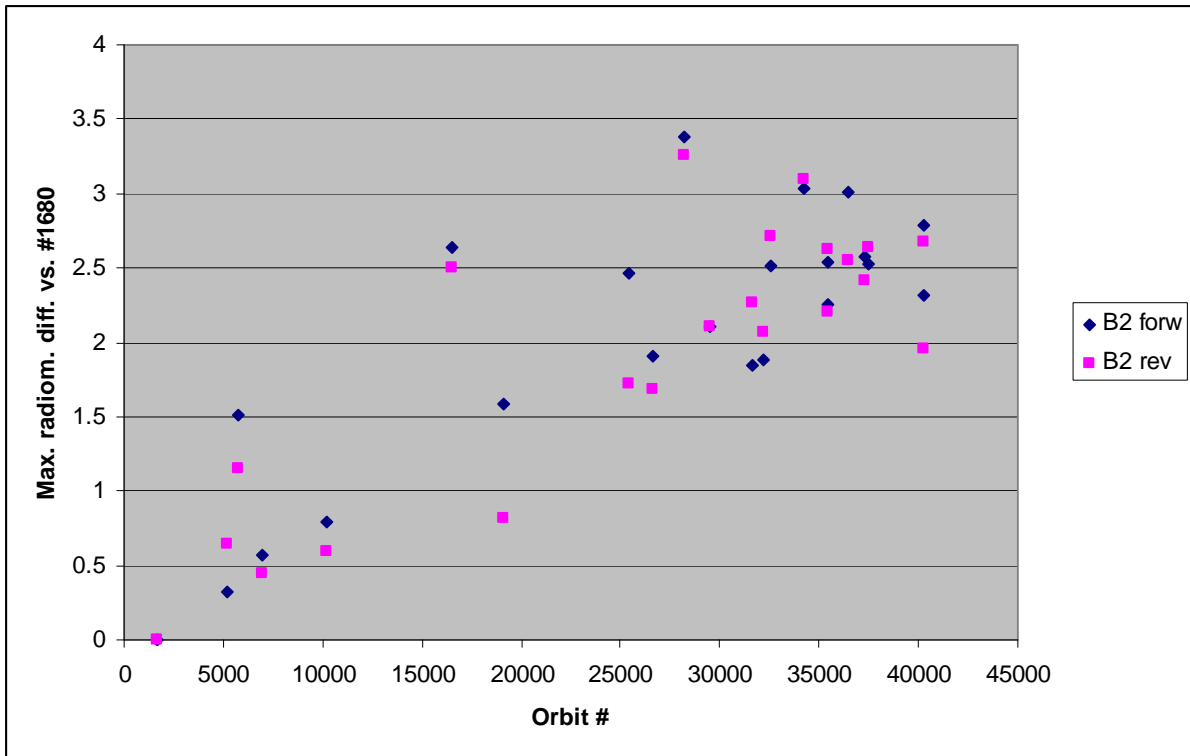


Figure 30. B2. Maximum radiometric differences to orbit #1680 vs. orbit number.

11 Further data reduction

The analysis shown so far gives detector characterisation snapshots at the times of the IF16 recordings. These data are contaminated by outliers and statistical errors. Anyway, for level 1 correction the data cannot be used directly. A single correction data set for the whole mission would lead to inconsistent level 1 products with radiometric differences up to 4%. Thus, a further data reduction is mandatory to make the non-linearity correction applicable throughout the mission. Furthermore, this data reduction improves the statistics. Especially forward/reverse non-linearity correction requires a common treatment. Otherwise statistically induced forward/reverse differences are produced.

The concept introduced is a multidimensional linear regression of DCnlin vs. DClin for forward and reverse combined with respect to orbit number, ice absorption and instrument temperature. The advantage of DCnlin over ADCmaxmin is that DCnlin is specific for the detector but not for the sweep direction. The ADCmaxmin values are affected by the digitisation of the interferogram and are thus different for forward and reverse.

The text file with all fit outputs is read in and the quadratic and cubic (only A1 and A2) non-linearity coefficients are extracted. The non-linearity curves are built for 6000 points with the DClin spaced in increments of 10. For each of the 6000 points a complete linear regression with respect to orbit number, instrument temperature, and peak ice absorption is carried out. Regression coefficients are obtained allowing calculating DCnlin. The standard deviation in the DCnlin domain is calculated and data sets (defined by orbit, channel, sweep direction) where the DCnlin residual exceeds twice the standard deviation are marked as outliers and discarded in the second regression round. It was ensured that outliers are related indeed to a specific orbit, channel, sweep direction and thus appear in all 6000 data points.

Detector curves for conditions of the IF16 measurements are calculated from the regression data and the DCnlin values for the respective interferograms used in the fit calculated. This requires to load the data and to apply the DCzero method for each data set. The DCnlin to ADCmaxmin

polynomial is fitted and then used to fit the BOMEM parameters. Since these polynomials refer to ADCmaxmin values which are different for forward and reverse due to digitisation the BOMEM parameters are again sweep direction dependent. Radiometric differences with respect to orbit 1680 were formed and can be found in Tables 4a and b.

In most cases the differences between regression and single fit differences are within 0.5%. When furthermore accepting differences above 0.5% where a forward/reverse single fit difference of more than 0.5% occurred the percentage of good data is: A1 forward 74%, A1 reverse 74%, A2 forward 89%, A2 reverse 84%, B1 forward 68%, B1 reverse 79%, B2 forward 74%, B2 reverse 74%. From these numbers we conclude that the regression does a good job, harmonises the data and does not introduce large systematic errors. Care should be taken, however, for orbits with large ice contamination since the available IF16 data with significant ice amount are very rare. Furthermore, in case of heavy ice absorption the peak absorption value is not a good figure of merit since the scattering changes the spectral shape significantly. Anyhow, there are only two short time periods with large ice contamination during the mission.

In the final step correction factors for all IF16 orbits are calculated from the BOMEM parameters obtained from the regression analysis. The ADCmaxmin are defined in steps of 10 from 10000 to 42000. A linear regression of the correction factors is carried out for each ADCmaxmin value with respect to orbit number, temperature and ice peak absorption and the regression coefficients were tabulated. A small software tool was made which calculates BOMEM parameters from these coefficients as function of orbit number, instrument temperature and ice peak absorption. These values serve as input for the aux file for level 1 processing. Radiometric differences introduced by the last regression were tested to be negligible. This is no surprise since no further averaging is introduced.

It is interesting to compare the current non-linearity correction with the new one. Of course, the intercomparison is based on radiometric differences. Furthermore, the difference was also expressed in terms of radiance offset as defined in section "*Radiance contrast difference*". Figures 31 to 34 show the differences for orbit 1680 for all channels forward and reverse. The maximum radiometric differences for all IF16 orbits are summarised in Table 5. The on-ground detector characterisation used in the current level 1 processing is basically in line with the current results. The maximum differences are within 3%. For channel A1 the maximum differences were at the start of the mission and decreases towards the end. For channel A2 the differences were moderate at the beginning changed sign and are now getting larger. For B1 throughout the mission the differences are within 1%. For B2 the same holds as for A2.

Table 4a. Maximum radiometric differences from single fits and regression results. Channels A1, A2

#	Date	Tinst			Ice absorption/%	A2 Gain(#1680/#x)	A1						A2								
							forward			reverse			forw-rev separate fit	forward			reverse			forw-rev separate fit	
							% diff. max. wrt. #1680	% diff. max. wrt. #1680	regression-separate fit	% diff. max. wrt. #1680	% diff. max. wrt. #1680	regression-separate fit		% diff. max. wrt. #1680	% diff. max. wrt. #1680	regression-separate fit	% diff. max. wrt. #1680	% diff. max. wrt. #1680	regression-separate fit		
1680	26.06.2002	220.24	218.68	223.53	0	1.00	0.00	0.00	0.00	0.00	0.00	0.00	0.00	0.00	0.00	0.00	0.00	0.00	0.00	0.00	0.00
5203	27.02.2003	213.07	211.68	218.31	15	1.01	-0.03	0.69	0.72	-0.49	0.49	0.98	0.46	-0.27	-0.09	0.18	-0.06	0.08	0.14	-0.21	-0.21
5764	07.04.2003	218.98	217.55	221.42	-4	1.00	-0.12	0.20	0.32	1.18	0.13	-1.05	-1.30	0.21	0.22	0.01	1.58	0.23	-1.35	-1.37	-1.37
6990	02.07.2003	220.43	218.92	223.84	1	1.00	-0.06	0.31	0.37	-0.62	0.30	0.92	0.56	0.16	0.27	0.11	1.04	0.31	-0.73	-0.88	-0.88
10230	13.02.2004	216.14	214.64	220.96	-4	0.95	-0.07	0.46	0.53	0.07	0.56	0.49	-0.14	0.40	0.49	0.09	0.45	0.36	-0.09	-0.05	-0.05
16486	25.04.2005	224.22	222.94	227.91	53	0.85	-0.87	0.53	1.40	1.57	0.55	-1.02	-2.44	2.59	1.83	-0.76	2.27	1.61	-0.66	0.32	0.32
19146	28.10.2005	222.51	221.14	225.99	5	0.90	0.18	0.90	0.72	0.41	1.02	0.61	-0.23	0.44	1.35	0.91	0.29	1.24	0.95	0.15	0.15
25426	10.01.2007	217.17	215.86	223.03	-4	0.87	0.97	1.12	0.15	1.16	1.33	0.17	-0.19	1.87	1.52	-0.35	1.79	1.29	-0.50	0.08	0.08
26589	01.04.2007	220.52	219.15	225.18	-3	0.87	0.82	1.15	0.33	0.85	1.29	0.44	-0.03	1.41	1.66	0.25	1.50	1.55	0.05	-0.09	-0.09
28179	21.07.2007	223.42	221.90	227.81	-2	0.84	0.77	1.09	0.32	1.45	1.25	-0.20	-0.68	2.90	2.02	-0.88	2.33	1.83	-0.50	0.57	0.57
29538	24.10.2007	222.85	221.52	226.28	-4	0.85	0.93	1.18	0.25	0.98	1.38	0.40	-0.05	1.89	2.03	0.14	2.03	1.83	-0.20	-0.14	-0.14
31671	21.03.2008	219.58	218.26	224.70	0	0.85	0.80	1.44	0.64	0.59	1.61	1.02	0.21	1.95	2.01	0.06	1.55	1.77	0.22	0.40	0.40
32229	29.04.2008	223.94	222.56	228.48	2	0.82	-0.52	1.37	1.89	1.06	1.58	0.52	-1.58	2.77	2.28	-0.49	1.93	2.13	0.20	0.84	0.84
32547	21.05.2008	226.76	225.32	229.44	-4	0.83	0.29	1.18	0.89	0.39	1.43	1.04	-0.10	2.64	2.42	-0.22	2.62	2.17	-0.45	0.02	0.02
34276	19.09.2008	222.46	221.18	226.71	1	0.82	1.34	1.45	0.11	1.55	1.63	0.08	-0.21	2.54	2.39	-0.15	2.46	2.16	-0.30	0.08	0.08
35406	07.12.2008	221.56	220.29	225.94	-3	0.82	1.25	1.49	0.24	1.40	1.71	0.31	-0.15	2.44	2.29	-0.15	2.12	2.06	-0.06	0.32	0.32
36480	20.02.2009	216.52	215.11	223.27	-2	0.82	1.25	1.67	0.42	1.53	1.87	0.34	-0.28	2.49	2.13	-0.36	2.41	1.89	-0.52	0.08	0.08
37339	21.04.2009	223.18	221.71	227.76	0	0.80	1.26	1.54	0.28	1.61	1.79	0.18	-0.35	2.61	2.60	-0.01	2.38	2.35	-0.03	0.23	0.23
37469	30.04.2009	224.51	223.13	227.76	0	0.80	1.27	1.61	0.34	1.46	1.81	0.35	-0.19	2.53	2.54	0.01	2.01	2.36	0.35	0.52	0.52
40274	12.11.2009	223.75	222.50	226.77	-4	0.82	1.51	1.67	0.16	1.28	1.90	0.62	0.23	2.66	2.65	-0.01	2.40	2.40	0.00	0.26	0.26

separate fits

nlin curve regression

orbit 16486: % diff. calculated for much smaller ADCmaxmin from orbit with max. ice contamination

Table 4b. Maximum radiometric differences from single fits and regression results. Channels B1, B2

#	Date	Tinst			Ice absorption/%	A2 Gain(#1680/#x)	B1						B2							
							forward			reverse			forward			reverse				
							% diff. max. wrt. #1680	% diff. max. wrt. #1680	regression-separate fit	% diff. max. wrt. #1680	% diff. max. wrt. #1680	regression-separate fit	forw-rev separate fit	% diff. max. wrt. #1680	% diff. max. wrt. #1680	regression-separate fit	% diff. max. wrt. #1680	% diff. max. wrt. #1680	regression-separate fit	forw-rev separate fit
1680	26.06.2002	220.24	218.68	223.53	0	1.00	0.00	0.00	0.00	0.00	0.00	0.00	0.00	0.00	0.00	0.00	0.00	0.00	0.00	0.00
5203	27.02.2003	213.07	211.68	218.31	15	1.01	0.37	0.31	-0.06	-0.06	0.38	0.44	0.43	0.32	0.60	0.28	0.65	0.68	0.03	-0.33
5764	07.04.2003	218.98	217.55	221.42	-4	1.00	0.69	-0.02	-0.71	0.14	0.08	-0.06	0.55	1.51	0.22	-1.29	1.15	0.27	-0.88	0.36
6990	02.07.2003	220.43	218.92	223.84	1	1.00	-0.41	0.19	0.60	-0.10	0.20	0.30	-0.31	0.57	0.38	-0.19	0.44	0.41	-0.03	0.13
10230	13.02.2004	216.14	214.64	220.96	-4	0.95	-0.47	0.25	0.72	-0.63	0.13	0.76	0.16	0.79	0.56	-0.23	0.59	0.47	-0.12	0.20
16486	25.04.2005	224.22	222.94	227.91	53	0.85	1.30	1.06	-0.24	0.70	1.01	0.31	0.60	2.64	1.82	-0.82	2.50	1.78	-0.72	0.14
19146	28.10.2005	222.51	221.14	225.99	5	0.90	-0.53	0.70	1.23	-0.95	0.57	1.52	0.42	1.59	1.36	-0.23	0.82	1.28	0.46	0.77
25426	10.01.2007	217.17	215.86	223.03	-4	0.87	0.55	0.74	0.19	0.30	0.60	0.30	0.25	2.47	1.62	-0.85	1.72	1.58	-0.14	0.75
26589	01.04.2007	220.52	219.15	225.18	-3	0.87	0.37	0.81	0.44	0.20	0.62	0.42	0.17	1.91	1.70	-0.21	1.69	1.61	-0.08	0.22
28179	21.07.2007	223.42	221.90	227.81	-2	0.84	1.54	0.81	-0.73	1.27	0.68	-0.59	0.27	3.38	1.85	-1.53	3.26	1.77	-1.49	0.12
29538	24.10.2007	222.85	221.52	226.28	-4	0.85	0.73	0.87	0.14	0.81	0.73	-0.08	-0.08	2.11	1.89	-0.22	2.10	1.83	-0.27	0.01
31671	21.03.2008	219.58	218.26	224.70	0	0.85	0.43	1.04	0.61	0.91	0.90	-0.01	-0.48	1.85	2.12	0.27	2.27	2.10	-0.17	-0.42
32229	29.04.2008	223.94	222.56	228.48	2	0.82	-0.02	1.06	1.08	0.31	0.87	0.56	-0.33	1.88	2.19	0.31	2.07	2.11	0.04	-0.19
32547	21.05.2008	226.76	225.32	229.44	-4	0.83	0.73	0.96	0.23	0.56	0.82	0.26	0.17	2.52	2.08	-0.44	2.71	2.02	-0.69	-0.19
34276	19.09.2008	222.46	221.18	226.71	1	0.82	1.14	1.11	-0.03	0.83	0.95	0.12	0.31	3.03	2.32	-0.71	3.10	2.28	-0.82	-0.07
35406	07.12.2008	221.56	220.29	225.94	-3	0.82	0.63	1.09	0.46	0.57	0.94	0.37	0.06	2.54	2.30	-0.24	2.21	2.26	0.05	0.33
36480	20.02.2009	216.52	215.11	223.27	-2	0.82	1.10	1.13	0.03	0.98	0.97	-0.01	0.12	3.01	2.41	-0.60	2.55	2.36	-0.19	0.46
37339	21.04.2009	223.18	221.71	227.76	0	0.80	1.02	1.20	0.18	0.76	1.02	0.26	0.26	2.58	2.49	-0.09	2.41	2.45	0.04	0.17
37469	30.04.2009	224.51	223.13	227.76	0	0.80	0.78	1.19	0.41	0.67	1.06	0.39	0.11	2.53	2.49	-0.04	2.64	2.49	-0.15	-0.11
40274	12.11.2009	223.75	222.50	226.77	-4	0.82	0.96	1.23	0.27	0.87	1.10	0.23	0.09	2.79	2.59	-0.20	2.67	2.59	-0.08	0.12

separate fits

nlin curve regression

orbit 16486: % diff. calculated for much smaller ADCmaxin from orbit with max. ice contamination

Table 5. Maximum radiometric differences from regression results and current level 1

#	Date	Tinst			Ice absorption/%	Gain(#1680/#x)	% diff. max. regression - current L1							
							A1		A2		B1		B2	
							forward	reverse	forward	reverse	forward	reverse	forward	reverse
1680	26.06.2002	220.24	218.68	223.53	0	1.00	-2.30	-2.34	-0.93	-0.98	-0.78	-0.88	-0.68	-0.83
5203	27.02.2003	213.07	211.68	218.31	15	1.01	-1.60	-1.84	-1.01	-0.95	-0.47	-0.51	-0.08	-0.15
5764	07.04.2003	218.98	217.55	221.42	-4	1.00	-2.10	-2.22	-0.70	-0.74	-0.76	-0.81	-0.46	-0.56
6990	02.07.2003	220.43	218.92	223.84	1	1.00	-1.99	-2.03	-0.65	-0.67	-0.59	-0.68	-0.30	-0.42
10230	13.02.2004	216.14	214.64	220.96	-4	0.95	-1.84	-1.77	-0.44	-0.61	-0.53	-0.75	-0.12	-0.36
16486	25.04.2005	224.22	222.94	227.91	53	0.85	-0.26	-0.11	1.14	0.93	0.36	0.23	1.28	1.14
19146	28.10.2005	222.51	221.14	225.99	5	0.90	-1.38	-1.29	0.43	0.27	0.09	-0.31	0.69	0.46
25426	10.01.2007	217.17	215.86	223.03	-4	0.87	-1.17	-1.01	0.61	0.32	0.08	-0.28	0.95	0.76
26589	01.04.2007	220.52	219.15	225.18	-3	0.87	-1.14	-1.04	0.75	0.59	0.15	-0.26	1.03	0.79
28179	21.07.2007	223.42	221.90	227.81	-2	0.84	-1.19	-1.08	1.11	0.87	0.15	-0.19	1.18	0.96
29538	24.10.2007	222.85	221.52	226.28	-4	0.85	-1.10	-0.97	1.12	0.87	0.18	-0.15	1.22	1.01
31671	21.03.2008	219.58	218.26	224.70	0	0.85	-0.88	-0.79	1.11	0.81	0.33	0.10	1.45	1.29
32229	29.04.2008	223.94	222.56	228.48	2	0.82	-0.93	-0.78	1.38	1.17	0.33	0.07	1.52	1.30
32547	21.05.2008	226.76	225.32	229.44	-4	0.83	-1.09	-0.90	1.52	1.21	0.27	-0.06	1.41	1.21
34276	19.09.2008	222.46	221.18	226.71	1	0.82	-0.86	-0.76	1.48	1.21	0.38	0.14	1.65	1.47
35406	07.12.2008	221.56	220.29	225.94	-3	0.82	-0.82	-0.71	1.38	1.10	0.35	0.14	1.63	1.45
36480	20.02.2009	216.52	215.11	223.27	-2	0.82	-0.72	-0.64	1.22	0.93	0.39	0.15	1.75	1.55
37339	21.04.2009	223.18	221.71	227.76	0	0.80	-0.79	-0.63	1.69	1.39	0.46	0.19	1.83	1.64
37469	30.04.2009	224.51	223.13	227.76	0	0.80	-0.71	-0.60	1.64	1.40	0.45	0.22	1.83	1.67
40274	12.11.2009	223.75	222.50	226.77	-4	0.82	-0.66	-0.54	1.75	1.45	0.48	0.26	1.93	1.78

orbit 16486: % diff. calculated for much smaller ADCmaxmin from orbit with max. ice contamination

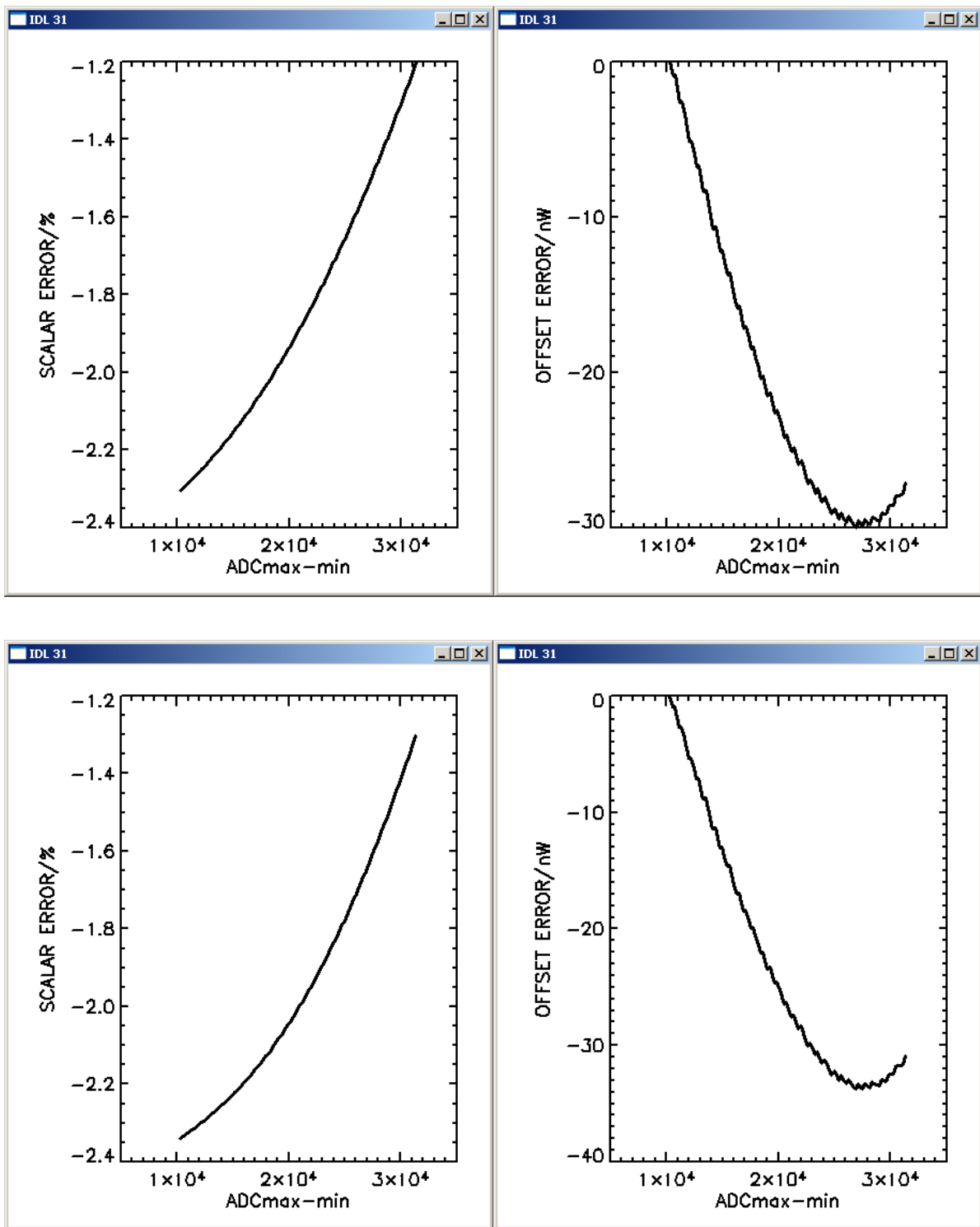


Figure 31. Orbit 1680, A1. Radiometric differences to current level 1. Top: forward, Bottom: reverse.

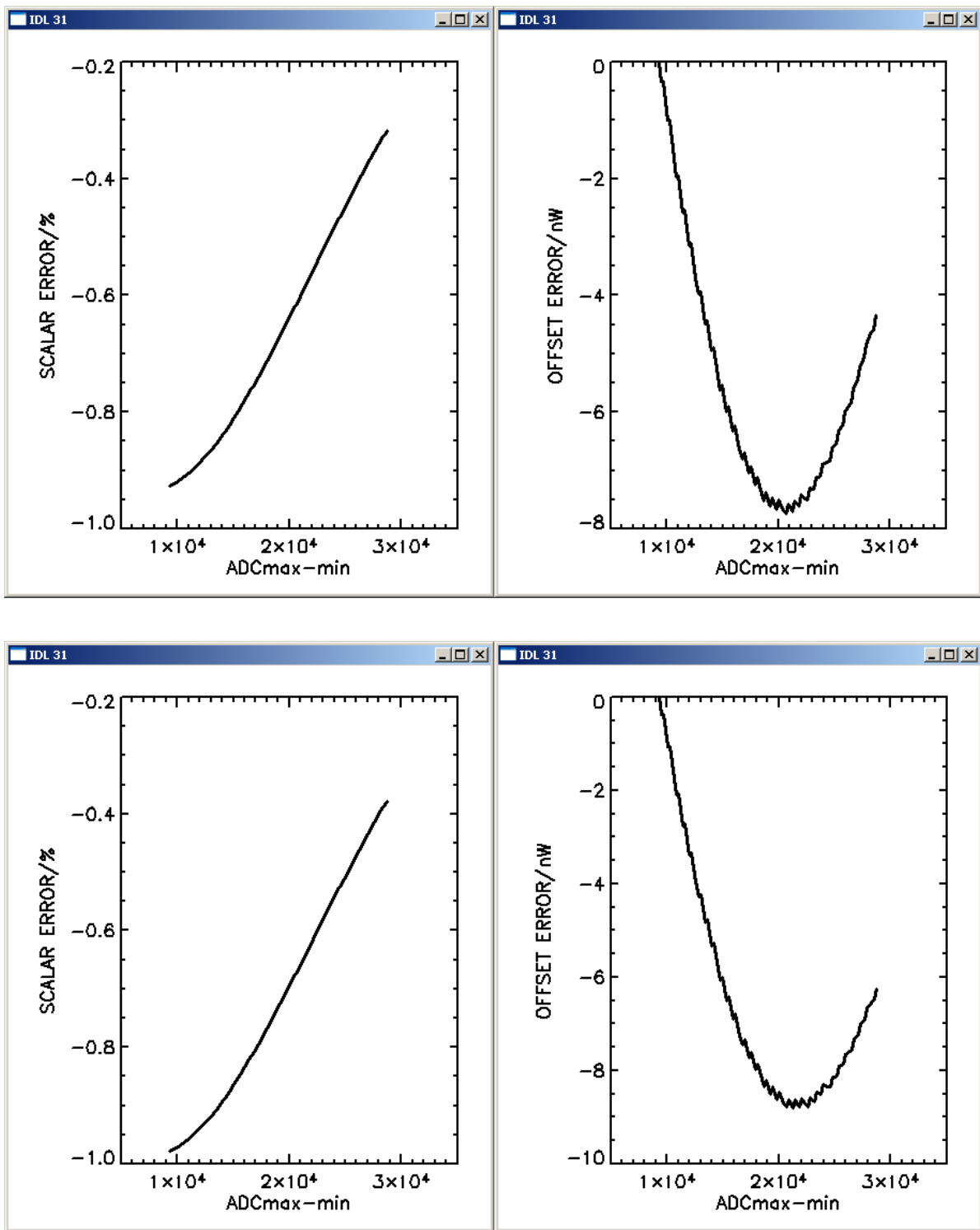


Figure 32. Orbit 1680, A2. Radiometric differences to current level 1. Top: forward, Bottom: reverse.

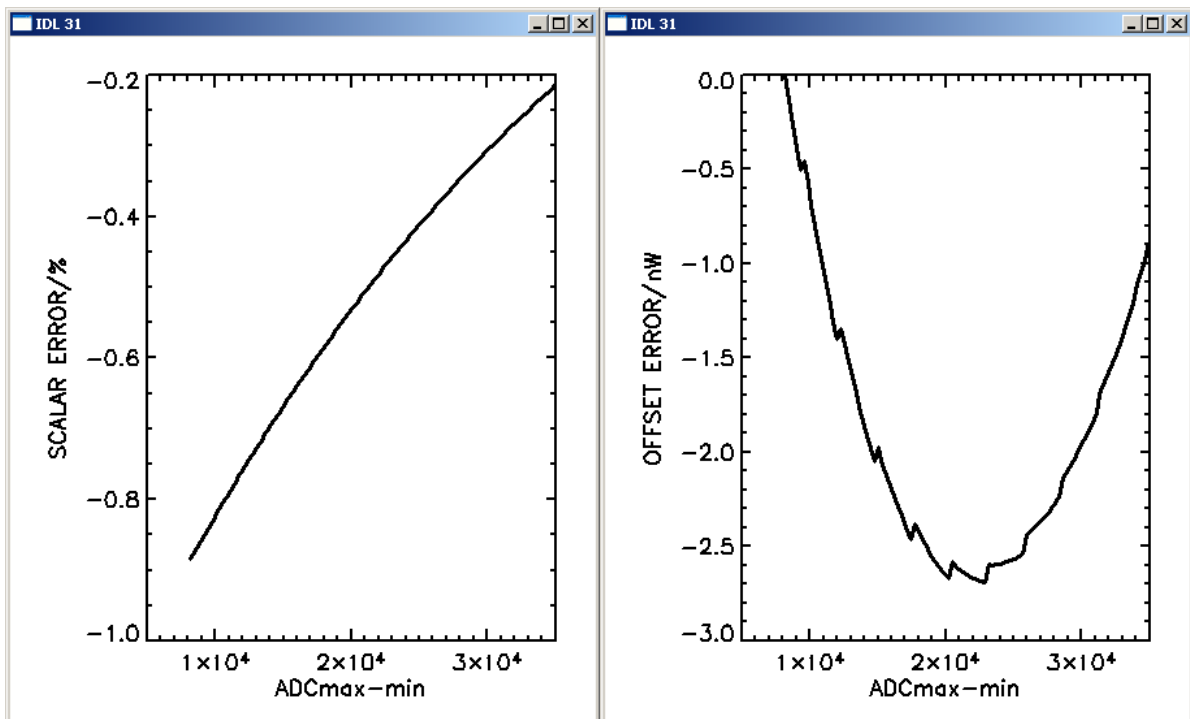
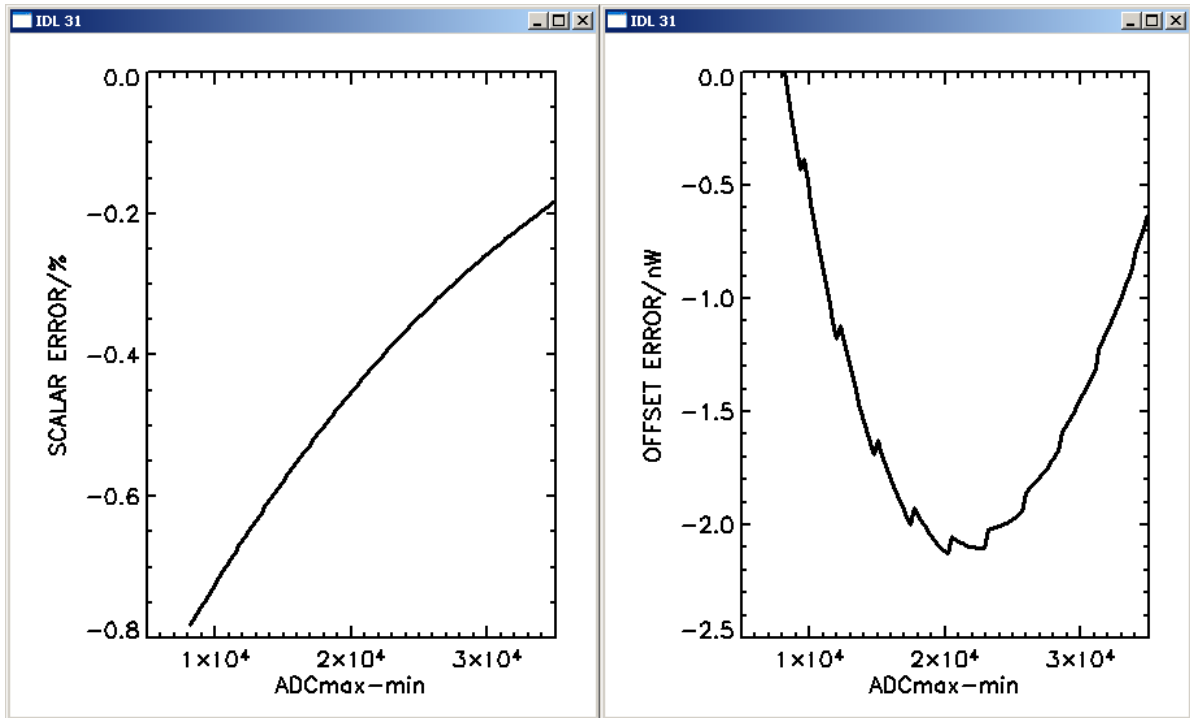


Figure 33. Orbit 1680, B1. Radiometric differences to current level 1. Top: forward, Bottom: reverse.

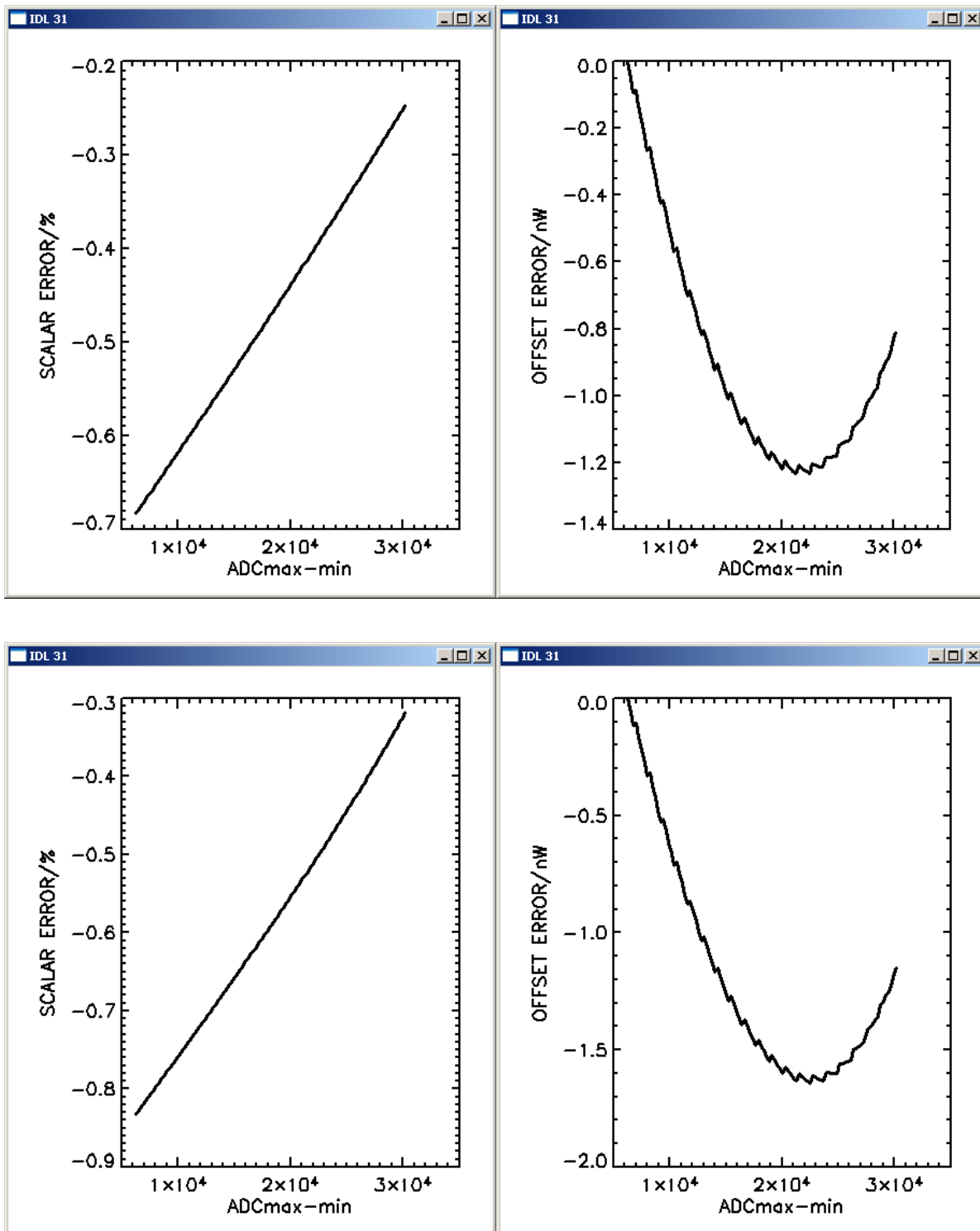


Figure 34. Orbit 1680, B2. Radiometric differences to current level 1. Top: forward, Bottom: reverse.

12 Error analysis

The following error sources have to be considered:

- Error due to modulation efficiency
- Intrinsic model error
- Out-of-band selection error

- Regression error
- ADCmaxmin error

12.1 Error due to modulation efficiency

The maximum error of 1.5% for A2 and 1% for all other channels was found (see chapter “Fits of all available IF4/IF16 sequences”). This error is common to all orbits. It is a great advantage of the IF16 fit to input the modulation efficiency. In case of IF16/IF4 fits a large scatter between orbits would have occurred.

12.2 Intrinsic model error

Parameterising the detector curve with quadratic or quadratic+cubic term is arbitrary. The investigations carried out for B1 show an effect on the order of 0.5%. For A1 and A2 with quadratic and cubic term the error should be even smaller. To be conservative 0.5% error was assumed for all channels.

12.3 Out-of-band selection error

The few samples investigated show incoherent results (see section “Dependence on out-of-band artifacts”). From the current state of the investigation no error was added.

12.4 Regression error

The linear regression certainly contains a rather crude assumption of linear behaviour of the detector curves from instrument temperature, ice contamination, and orbit number. Anyway, the radiometric errors beside large ice contamination were found to be within 0.5% (see chapter “Further data reduction”).

12.5 ADCmaxmin error

The inputs for non-linearity correction to level 1 processing are ADCmaxmin values. They are defined on the non-linear domain of the detector curve and furthermore have systematic errors due to sampling, phase errors, and spectral shape (the minimum of the interferogram is influenced by the spectral shape). The interferogram minimum contains very low resolution information and should show the largest difference between CBB and low tangent scenes. As described in [RD2] the ADCmaxmin are related to the DCnlin via a quadratic polynomial. An example is shown in Table 6. The deviations of the ADCmaxmin from the polynomial are the only origin for systematic errors of the method. As can be seen in the table the observed-calculated (OMC) are very small. The code for calculating the radiometric difference between two sets of non-linearity correction parameters was modified to accommodate the same curve with altered and unaltered ADCmaxmin and calculate the scalar difference. The OMCs of CBB, DS, and the scenes were used to alter the ADCmaxmin values. The resulting influence was found to be negligible. This is good news since the level 1 processing does not need to be modified.

Table 6. DCnlin to ADCmaxmin. Orbit #1680, A1 forward

File name	Tangent height/km	ADCmaxmin	OMC	DCnlin
-----------	-------------------	-----------	-----	--------

M2_1680Scn-igm-A1.14_IF16_RAW_SCE_0_	19.4	37701	12	36788
M2_1680_BB-igm-A1.0_IF16_RAW_DS_0_		10972	-39	10008
M2_1680_BB-igm-A1.60_IF16_RAW_CBB_0_		41396	12	40823
M2_1680Scn-igm-A1.37_IF16_RAW_SCE_0_	37.0	18631	21	17281
M2_1680Scn-igm-A1.39_IF16_RAW_SCE_0_	31.2	21154	24	19740
M2_1680Scn-igm-A1.41_IF16_RAW_SCE_0_	25.5	24007	-21	22519
M2_1680Scn-igm-A1.43_IF16_RAW_SCE_0_	20.1	31703	-47	30351
M2_1680Scn-igm-A1.53_IF16_RAW_SCE_0_	40.3	17423	41	16138
M2_1680Scn-igm-A1.55_IF16_RAW_SCE_0_	34.5	20040	10	18637
M2_1680Scn-igm-A1.57_IF16_RAW_SCE_0_	28.7	22900	-3	21435
M2_1680Scn-igm-A1.59_IF16_RAW_SCE_0_	23.2	26382	-11	24916

$$DCnlin = 322.17508 + 0.85279667 \times ADCmaxmin + 3.0258667e-006 \times ADCmaxmin^2$$

13 Proposal for level 2 quality check

- Calculate residuals for opaque ozone and CO2 regions (broad band) and check consistency of residuals throughout mission for old and new non-linearity correction (non-noise residuals may be due to spectroscopic errors, horizontal gradients)
- Compare retrieval results from A1 and A2 separately with old and new non-linearity correction
- Compare fitted temperatures with other data sources (radiosondes etc) and check time evolution of BIAS for old and new nonlinearity data.
- Compare ozone with NDSC and check time evolution of BIAS for old and new nonlinearity data.
- Compare species measured with non-linear and linear channels and check time evolution of BIAS for old and new nonlinearity data.

14 Summary

Based on previous work ([RD1], [RD2]) an in-flight non-linearity characterisation method was developed requiring modulation efficiencies from IF4/IF16 fits. The new method has been thoroughly investigated and tuned. All available IF16 sets were analysed and allowed to detect all parameters influencing detector non-linearity. The largest influence was found to be due to the aging of the photoconductive detectors. The maximum percentage radiance change is smaller than 4% among all orbits and channels. A linear regression was used for further data reduction and to allow calculating non-linearity correction parameters for any orbit in the mission. Only three parameters are necessary: orbit number, instrument temperature and peak

ice absorption. The combined maximum error for radiance contrast is 2.5% for A2 and 2% for all other channels. The error decreases with increasing integral photon flux. For high tangent height the error is 1.5% and decreases to half of that or less at low tangent height. The radiance contrast error of the current level 1 is below 3%. The advantage of the new in-flight characterisation is that the radiance accuracy is improved and consistent throughout the mission.